themselves in an autocrine manner or act on mesangial cells as a GBM-bound form, through integrin complexes on these cells.

Podocytes are terminally differentiated, quiescent cells, possessing well-developed processes, and express podocyte-specific proteins such as WT1 and synaptopodin (27). In contrast, typical "dedifferentiated" podocytes proliferate and have decreased synaptopodin expression (17). Abnormal podocyte function, such as dedifferentiation, loss, or inflammatory change, is postulated to play a central role in nephron degeneration (17). Therefore it is important to understand the underlying mechanisms, but very few factors are known to be involved in the maintenance of podocytes at differentiated phenotypes (7, 12, 21, 36). In this study, we revealed that CCN1 upregulates synaptopodin expression in vitro and showed that CCN1 is induced in vivo at the capillary loop stage, when synaptopodin is first detected during kidney development. Synaptopodin is essential for podocyte foot process formation, by blocking the actin-branching activity of α-actinin-4 to develop unbranched actin bundles (1). Our observation that CCN1 upregulated synaptopodin, but not α-actinin-4, implies the role of CCN1 in podocyte foot process formation, which needs to be clarified in the future studies.

CKIs maintain G0/G1 cell cycle arrest in mature podocytes, and their downregulation is responsible for podocyte proliferation in pathological conditions (5, 25, 34). We showed in this study that CCN1 enhances the expression of CKI p27 in vitro and that CCN1 is upregulated in vivo at the capillary loop stage, when p27 is also induced in the developing kidney (5, 25). Decreased CCN1 expression at podocytes in IgAN may contribute to downregulation of podocyte p27, as reported previously in proliferative IgAN (29).

A decrease in the ratio of CCN1-positive cells to WT1-positive cells was prominent in IgAN, indicating the appearance of CCN1-negative podocytes in IgAN. In fact, CCN1-negative podocytes were frequently observed in IgAN. CCN1-negative podocytes may contribute to the pathological lesion seen in IgAN in two ways: first, a decrease in GBM-bound CCN1 may enhance mesangial migration, which leads to glomerular tuft occlusion and to glomerulosclerosis. Second, excessive podocyte migration can lead to podocyte bridging, and further on to glomerular crescent formation (17, 20, 23, 26, 30, 31). The functional significance of CCN1 downregulation in IgAN should await further clarification.

Downregulation of CCN1 at podocytes may be merely a consequence of podocyte loss or damage, but we assume it unlikely for the following reasons. First, we found that WT1 expression intensity was not altered despite a dramatic change in CCN1 expression in podocytes. Second, a reduction in CCN1 expression at podocytes was significant in IgAN, DN, and MN compared with MCNS and FSGS. Since MCNS and FSGS are supposed to have more pronounced podocyte damage compared with IgAN (15), it is unlikely that podocyte damage alone leads to CCN1 downregulation. Third, the findings that podocyte CCN1 expression is decreased in glomeruli with overt mesangial expansion, and that CCN1 is markedly downregulated at podocytes adjacent to mesangial expansion or segmental sclerosis, supports the possible mesangial-repellent activity of CCN1. Taken together, we hypothesize that decreased CCN1 expression in podocytes may, at least in part, play a role in disease progression in these glomerulopathies.

In conclusion, we show that CCN1, which acts as a potential mesangial-repellent factor and a podocyte differentiation factor, is predominantly expressed by podocytes in glomeruli of adult human kidneys and that CCN1 expression at podocytes is downregulated in various diseases associated with mesangial expansion. Although the functional relevance is still unclarified, these findings raise the possibility that impairment of CCN1 expression at podocytes may play a role in the progression of various human glomerulopathies.

ACKNOWLEDGMENTS

The authors gratefully acknowledge Dr. Peter Mundel (Mount Sinai School of Medicine, New York, NY) for the immortalized mouse podocyte cell line and Dr. Peter W. Mathieson (University of Bristol, Bristol, UK) for the immortalized human podocyte cell line; Dr. Lester F. Lau (University of Illinois at Chicago) and Dr. K. Nagahama for discussions; C. Uwabe, J. Nakamura, and S. Saito for technical assistance; and A. Sonoda and S. Doi for secretarial assistance. We also acknowledge the contribution of collaborating obstetricians.

GRANTS

This work was supported in part by research grants from the Japanese Ministry of Education, Culture, Sports, Science and Technology and the Japanese Ministry of Health, Labour, and Welfare.

REFERENCES

1. **Asanuma K, Kim K, Oh J, Giardino L, Chabanis S, Faul C, Reiser J, Mundel P.** Synaptopodin regulates the actin-bundling activity of alpha-actinin in an isoform-specific manner. *J Clin Invest* 115: 1188–1198, 2005.
2. **Babic AM, Kireeva ML, Kolesnikova TV, Lau LF.** CYR61, a product of a growth factor-inducible immediate early gene, promotes angiogenesis and tumor growth. *Proc Natl Acad Sci USA* 95: 6355–6360, 1998.
3. **Brigstock DR.** The connective tissue growth factor/cysteine-rich 61/nephroblastoma overexpressed (CCN) family. *Endocr Rev* 20: 189–206, 1999.
4. **Chen CC, Mo FE, Lau LF.** The angiogenic factor Cyr61 activates a genetic program for wound healing in human skin fibroblasts. *J Biol Chem* 276: 47329–47337, 2001.
5. **Combs HL, Shankland SJ, Setzer SV, Hudkins KL, Alpers CE.** Expression of the cyclin kinase inhibitor, p27kip1, in developing and mature human kidney. *Kidney Int* 53: 892–896, 1998.
6. **Eremina V, Cui S, Gerber H, Ferrara N, Haigh J, Nagy A, Ema M, Rossant J, Jothy S, Miner JH, Quaggin SE.** Vascular endothelial growth factor A signaling in the podocyte-endothelial compartment is required for mesangial cell migration and survival. *J Am Soc Nephrol* 17: 724–735, 2006.
7. **Griffin SV, Hiromura K, Pippin J, Petermann AT, Blonski MJ, Krofft R, Takahashi S, Kulkarni AB, Shankland SJ.** Cyclin-dependent kinase 5 is a regulator of podocyte differentiation, proliferation, and morphology. *Am J Pathol* 165: 1175–1185, 2004.
8. **Groffen AJ, Veerkamp JH, Monnens LA, van den Heuvel LP.** Recent insights into the structure and functions of heparan sulfate proteoglycans in the human glomerular basement membrane. *Nephrol Dial Transplant* 14: 2119–2129, 1999.
9. **Grzeszkiewicz TM, Kirschling DJ, Chen N, Lau LF.** CYR61 stimulates human skin fibroblast migration through integrin $\alpha_v\beta_5$ and enhances mitogenesis through integrin $\alpha_v\beta_3$ independent of its carboxyl-terminal domain. *J Biol Chem* 276: 21943–21950, 2001.
10. **Hafdi Z, Lesavre P, Nejjari M, Halbwachs-Mecarelli L, Droz D, Noel LH.** Distribution of alphavbeta3, alphavbeta5 integrins and the integrin associated protein–IAP (CD47) in human glomerular diseases. *Cell Adhes Commun* 7: 441–451, 2000.
11. **Hilfiker-Kleiner D, Kaminski K, Kaminska A, Fuchs M, Klein G, Podewski E, Grote K, Kiian I, Wollert KC, Hilfiker A, Drexler H.** Regulation of proangiogenic factor CCN1 in cardiac muscle: impact of ischemia, pressure overload, and neurohumoral activation. *Circulation* 109: 2227–2233, 2004.
12. **Hunt JL, Pollak MR, Denker BM.** Cultured podocytes establish a size-selective barrier regulated by specific signaling pathways and dem-

onstrate synchronized barrier assembly in a calcium switch model of junction formation. *J Am Soc Nephrol* 16: 1593–1602, 2005.
13. **Kireeva ML, Mo FE, Yang GP, Lau LF.** Cyr61, a product of a growth factor-inducible immediate-early gene, promotes cell proliferation, migration, and adhesion. *Mol Cell Biol* 16: 1326–1334, 1996.
14. **Kireeva ML, Lam SC, Lau LF.** Adhesion of human umbilical vein endothelial cells to the immediate-early gene product Cyr61 is mediated through integrin $\alpha_v\beta_3$. *J Biol Chem* 273: 3090–3096, 1998.
15. **Koop K, Eikmans M, Baelde HJ, Kawachi H, De Heer E, Paul LC, Bruijn JA.** Expression of podocyte-associated molecules in acquired human kidney diseases. *J Am Soc Nephrol* 14: 2063–2071, 2003.
16. **Koshikawa M, Mukoyama M, Mori K, Suganami T, Sawai K, Yoshioka T, Nagae T, Yokoi H, Kawachi H, Shimizu F, Sugawara A, Nakao K.** Role of p38 mitogen-activated protein kinase activation in podocyte injury and proteinuria in experimental nephrotic syndrome. *J Am Soc Nephrol* 16: 2690–2701, 2005.
17. **Kriz W, LeHir M.** Pathways to nephron loss starting from glomerular diseases: insights from animal models. *Kidney Int* 67: 404–419, 2005.
18. **Latinkic BV, O'Brien TP, Lau LF.** Promoter function and structure of the growth factor-inducible immediate early gene *cyr61*. *Nucleic Acids Res* 19: 3261–3267, 1991.
19. **Lau LF, Lam SC.** The CCN family of angiogenic regulators: the integrin connection. *Exp Cell Res* 248: 44–57, 1999.
20. **Le Hir M, Keller C, Eschmann V, Hahnel B, Hosser H, Kriz W.** Podocyte bridges between the tuft and Bowman's capsule: an early event in experimental crescentic glomerulonephritis. *J Am Soc Nephrol* 12: 2060–2071, 2001.
21. **Miner JH, Morello R, Andrews KL, Li C, Antignac C, Shaw AS, Lee B.** Transcriptional induction of slit diaphragm genes by Lmx1b is required in podocyte differentiation. *J Clin Invest* 109: 1065–1072, 2002.
22. **Mo FE, Muntean AG, Chen CC, Stolz DB, Watkins SC, Lau LF.** CYR61 (CCN1) is essential for placental development and vascular integrity. *Mol Cell Biol* 22: 8709–8720, 2002.
23. **Moeller MJ, Soofi A, Hartmann I, Le Hir M, Wiggins R, Kriz W, Holzman LB.** Podocytes populate cellular crescents in a murine model of inflammatory glomerulonephritis. *J Am Soc Nephrol* 15: 61–67, 2004.
24. **Mundel P, Reiser J, Zuniga Mejia Borja A, Pavenstadt H, Davidson GR, Kriz W, Zeller R.** Rearrangements of the cytoskeleton and cell contracts induce process formation during differentiation of conditionally immortalized mouse podocyte cell lines. *Exp Cell Res* 236: 248–258, 1997.
25. **Nagata M, Nakayama K, Terada Y, Hoshi S, Watanabe T.** Cell cycle regulation and differentiation in the human podocyte lineage. *Am J Pathol* 153: 1511–1520, 1998.
26. **Oyanagi A, Orikasa M, Kawachi H, Ito Y, Koike H, Gejo F, Shimizu F.** Crescent-forming mechanism in an irreversible Thy-1 model in rats. *Nephron* 89: 439–447, 2001.
27. **Pavenstadt H, Kriz W, Kretzler M.** Cell biology of the glomerular podocyte. *Physiol Rev* 83: 253–307, 2003.
28. **Perbal B.** CCN proteins: multifunctional signaling regulators. *Lancet* 363: 62–64, 2004.
29. **Qiu LQ, Sinniah R, Hong Hsu SI.** Downregulation of Bcl-2 by podocytes is associated with progressive glomerular injury and clinical indices of poor renal prognosis in human IgA nephropathy. *J Am Soc Nephrol* 15: 79–90, 2004.
30. **Rampino T, Gregorini M, Camussi G, Conaldi PG, Soccio G, Maggio M, Bottelli A, Dal Canton A.** Hepatocyte growth factor and its receptor Met are induced in crescentic glomerulonephritis. *Nephrol Dial Transplant* 20: 1066–1074, 2005.
31. **Reiser J, Oh J, Shirato I, Asanuma K, Hug A, Mundel TM, Honey K, Ishidoh K, Kominami E, Kreidberg JA, Tomino Y, Mundel P.** Podocyte migration during nephrotic syndrome requires a coordinated interplay between cathepsin L and α3 integrin. *J Biol Chem* 279: 34827–34832, 2004.
32. **Sawai K, Mori K, Mukoyama M, Sugawara A, Suganami T, Koshikawa M, Yahata K, Makino H, Nagae T, Fujinaga Y, Yokoi H, Yoshioka T, Yoshimoto A, Tanaka I, Nakao K.** Angiogenic protein Cyr61 is expressed by podocytes in anti-Thy-1 glomerulonephritis. *J Am Soc Nephrol* 14: 1154–1163, 2003.
33. **Sawai K, Mukoyama M, Mori K, Yokoi H, Koshikawa M, Yoshioka T, Takeda R, Sugawara A, Kuwahara T, Saleem MA, Ogawa O, Nakao K.** Redistribution of connexin43 expression in glomerular podocytes predicts poor renal prognosis in patients with type 2 diabetes and overt nephropathy. *Nephrol Dial Transplant* 21: 2472–2477, 2006.
34. **Shankland SJ, Eitner F, Hudkins KL, Goodpaster T, D'Agati V, Alpers CE.** Differential expression of cyclin-dependent kinase inhibitors in human glomerular disease: role in podocyte proliferation and maturation. *Kidney Int* 58: 674–683, 2000.
35. **Suganami T, Mukoyama M, Mori K, Yokoi H, Koshikawa M, Sawai K, Hidaka S, Ebihara K, Tanaka T, Sugawara A, Kawachi H, Vinson C, Ogawa Y, Nakao K.** Prevention and reversal of renal injury by leptin in a new mouse model of diabetic nephropathy. *FASEB J* 19: 127–129, 2005.
36. **Vaughan MR, Pippin JW, Griffin SV, Krofft R, Fleet M, Haseley L, Shankland SJ.** ATRA induces podocyte differentiation and alters nephrin and podocin expression in vitro and in vivo. *Kidney Int* 68: 133–144, 2005.
37. **Yang GP, Lau LF.** Cyr61, product of a growth factor-inducible immediate early gene, is associated with the extracellular matrix and the cell surface. *Cell Growth Differ* 2: 351–357, 1991.

Neutrophil gelatinase-associated lipocalin as the real-time indicator of active kidney damage

K Mori[1] and K Nakao[1]

[1]*Department of Medicine and Clinical Science, Kyoto University Graduate School of Medicine, Kyoto, Japan*

Neutrophil gelatinase-associated lipocalin (Ngal, 24p3, SIP24, lipocalin 2, or siderocalin) was originally purified from neutrophils, but with unknown function. Recently, it was identified that Ngal activates nephron formation in the embryonic kidney, is rapidly and massively induced in renal failure and possesses kidney-protective activity. We would like to propose that blood, urine, and kidney Ngal levels are the real-time indicators of active kidney damage, rather than one of many markers of functional nephron number (as Forest Fire Theory). Ngal is a novel iron-carrier protein exerting pleiotropic actions including the upregulation of epithelial marker E-cadherin expression, opening an exciting field in cell biology.

Kidney International (2007) **71,** 967–970. doi:10.1038/sj.ki.5002165; published online 7 March 2007

KEYWORDS: progression of renal failure; development; iron; siderophore; mesenchymal-epithelial transition; ischemia-reperfusion; gene expression

Correspondence: *K Mori, Department of Medicine and Clinical Science, Kyoto University Graduate School of Medicine, 54 Shogoin Kawahara-cho, Sakyo-ku, Kyoto 606-8507, Japan. E-mail: keyem@kuhp.kyoto-u.ac.jp*

Received 5 December 2006; revised 4 January 2007; accepted 9 January 2007; published online 7 March 2007

MOLECULAR STRUCTURE OF NGAL

Neutrophil gelatinase-associated lipocalin (Ngal) belongs to the lipocalin superfamily, which are secreted or cytosolic proteins with barrel-like structure, carrying hydrophobic ligands (such as fatty acids, retinoids, and pheromones) in their core pocket.[1] Recent works have elucidated the pathophysiological roles of lipocalins in energy homeostasis. Retinol-binding protein 4 impairs insulin signaling in muscles causing insulin resistance,[2] whereas lipocalin-type (or brain) prostaglandin D synthase (β-trace) inhibits insulin-stimulated proliferation of vascular smooth muscle cells resulting in protection against atherosclerosis.[3] Mice with a null mutation in adipocyte fatty acid-binding protein 4 or adipocyte protein 2 become obese under high-fat diet but do not develop insulin resistance.[4] Little is known about the involvement of the ligands in these metabolic activities of lipocalins. Goetz *et al.*[5] carried out an epoch work of the X-ray crystallography for recombinant human Ngal protein expressed in *Escherichia coli.* They demonstrated that the ligand for Ngal is siderophore. Siderophores are a diverse group of small (1 kDa or less) non-peptide iron (Fe^{3+})-binding chemicals produced in bacteria, fungi, and plants and their mammalian version remains to be identified.[6–9] Of note, XL1-Blue strain of *E. coli* synthesizes a siderophore called enterochelin (or enterobactin), but BL21 commonly used for recombinant protein expression does not make enterochelin.[5] Probably outside the pocket, Ngal binds with gelatinase B (matrix metalloproteinase-9 or type IV collagenase) and with hepatocyte growth factor and modulates their activity.[10–12]

NGAL IN KIDNEY DEVELOPMENT

Mammalian metanephric mesenchyme and ureteric bud coordinate a complicated interaction to develop themselves into mature nephrons.[13] Barasch *et al.*[14] established an organ culture system, where isolated rat metanephric mesenchyme converts into glomeruli and proximal tubules by stimulation with condition media prepared from a mouse ureteric bud cell line. Leukemia-inhibitory factor and Ngal were the epithelial inducers purified at the protein level using this assay.[14,15] Genetic inactivation of Ngal (by Flo *et al.*) or leukemia-inhibitory factor signal transducer gp130 does not result in agenesis of the kidney, indicating a high redundancy in nephrogenesis pathways.[14,16] Yang *et al.*[15] have shown that

mouse Ngal protein secreted from cultured ureteric bud cells possesses nephron-inducing activity and can also bind iron. Surprisingly, Ngal–bacterial siderophore–iron complex has much stronger activity than Ngal–siderophore (without iron) and apo-Ngal (without siderophore),[17] indicating the first example of 'siderophore-binding proteins,' in any species, dependent on the presence of iron for the biological activity.[7]

NGAL IN RENAL FAILURE

Recapture of genetic program of embryo is often observed in tissue injuries. Devarajan *et al.*[18,19] have analyzed animal models of acute renal failure to screen biomarkers useful in the clinical settings and to understand the molecular mechanisms of kidney injury, to begin with by use of microarray. Within a few hours, Ngal mRNA is highly upregulated after kidney injury, such as renal ischemia-reperfusion and cisplatin nephropathy, where Ngal induction precedes the elevation of classical markers for kidney damage: serum creatinine, urinary *N*-acetyl glucosaminidase, β 2-microglobulin levels.[19,20] Furthermore, Mori *et al.*[9] and other groups have reported that Ngal protein is abundantly accumulated in the blood, urine, and renal proximal and distal tubules in acute renal failure of humans: in cases associated with renal ischemia (sepsis, hypovolemia, and heart failure), nephrotoxin (antibiotics, cisplatin, bisphosphonate, nonsteroidal anti-inflammatory drugs, radiocontrast, and hemoglobinuria), kidney-parenchymal damage (glomerulonephrits, minimal change disease, focal segmental glomerulosclerosis, and diabetic nephropathy), hemolytic-uremic syndrome and posttransplant rejection. Mishra *et al.*[21] presented the clinical usefulness of blood and urinary Ngal as extremely early markers of acute kidney disease. As early as 1–2 h after the cardiopulmonary bypass surgery in children and in adults (with average bypass time of 2–3 h), the Ngal levels are dramatically and specifically elevated in those who are going to develop acute renal failure (diagnosed by more than 50% rise in the serum creatinine levels a few days later).[21,22] Acute worsening of chronic renal failure may be also predicted by elevated urinary Ngal levels (Nickolas T *et al.*, submitted). In general, to evaluate the severity of renal failure, at least two aspects should be considered (Figure 1): the ratio of functional versus atrophic nephrons (or the results of kidney injury) and the severity of on-going damage. Analogy may hold true for forest fire (Forest Fire Theory). We propose here that induction of Ngal expression is a real-time indicator of active renal injury.

Functional significance of Ngal upregulation in renal failure was investigated by Mori[9] and Mishra *et al.*,[23] who analyzed separate sets of animals. Single intraperitoneal or subcutaneous injection of recombinant Ngal protein into mice (Figure 2) significantly ameliorates kidney damage after renal ischemia-reperfusion injury, if Ngal is given before ischemia or 1 h after reperfusion. Berger *et al.*[24] generated Ngal knockouts and found no difference in renal damage at 24 h after renal ischemia-reperfusion compared with wild-type mice. Although Ngal mRNA upregulation is a rapid response, the speed and amount of endogenous Ngal induction may not be sufficient to show significant protection in this setting. Experiments in more chronic and milder models may give different results.

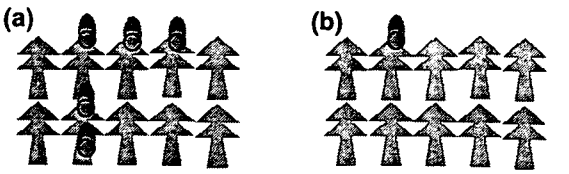

Figure 1 | Forest Fire Theory for worsening renal function. Forest (kidney) is composed of trees (nephrons). Both models (**a**) and (**b**) have 60% viable trees (shown in green) and 40% of trees are burnt down (shown in gray, corresponding to sclerosis of glomeruli, and atrophy of tubules). However, model (**a**) has much stronger fire (shown in red, that is ongoing nephron damage) than model (**b**). We propose that serum creatinine level or glomerular filtration rate is a marker for functional nephron numbers (green trees), whereas serum, urinary, or renal Ngal level indicates the extent of active lesion in the kidney (red fire in the forest).

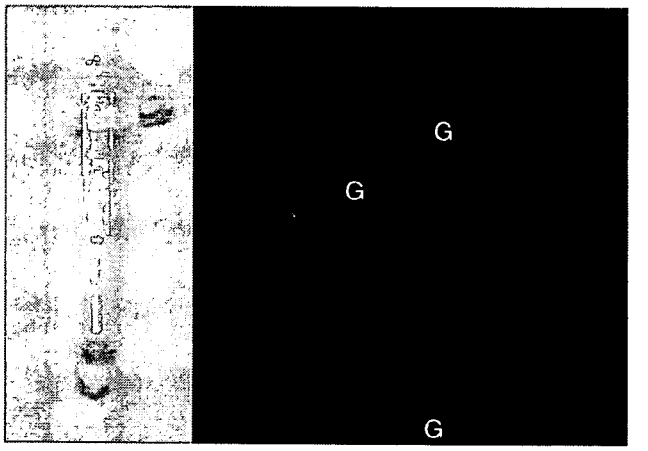

Figure 2 | Kidney protection by a red protein. Ngal protein shows a red color when ligated with iron and siderophore (left). Intravenous injection of A568-labeled Ngal (red fluorescence, right) into normal mice results in rapid glomerular (G) filtration and reabsorption by proximal tubules. Administration of iron-loaded Ngal protects the kidney from renal ischemia-reperfusion injury.

TRANSCRIPTIONAL REGULATION OF NGAL

Neutrophils,[25] monocytes/macrophages,[26] and adipocytes[27] are cells with abundant Ngal expression (Figure 3). Importantly, immature neutrophils (myelocytes and meta-myelocytes) have high expression level of Ngal mRNA, whereas mature neutrophils/granulocytes in the circulation have lost the mRNA but contain large amount of Ngal protein,[25] making it impossible to determine the involvement of neutrophil-derived Ngal in tissue injury by *in situ* mRNA hybridization. Ngal expression is highly induced not only in kidney injury, but also in epithelial inflammation of intestine,[28] skin and airway,[29] and in bacterial infection[16] and cancer.[30] Ngal inducers so far identified *in vitro* are

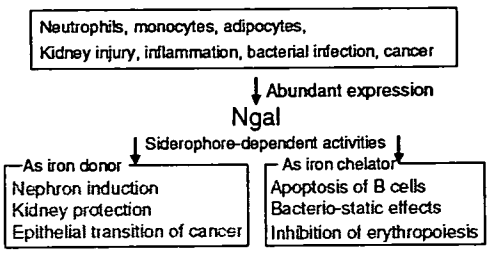

Figure 3 | Summary of expressional regulation and biological activities of Ngal.

IL-1β, tissue necrosis factor α, lipopolysaccharide, basic fibroblast growth factor, prostaglandin F2 α, phorbol ester, dexamethasone, retinoic acid, serum, and hypoxia.[20,26,29,31]

BIOLOGICAL ACTIVITY OF NGAL

Ngal exerts a broad range of biological activities (Figure 3). The coexistence of siderophore and iron is required not only for mesenchymal–epithelial transition of embryonic kidney[17] and oncogene Ras-transformed epithelial cells by Hanai *et al.*,[30] but also for kidney protection from renal failure by Mori *et al.*[9] In contrast, Ngal–siderophore complex without iron[17] (and potentially apo-Ngal)[32] can chelate iron from cells and iron deprivation is the mechanism for apoptosis of pro-B cells,[32,33] and for inhibition of bacterial growth and erythropoiesis.[5,16,34] Various other activities of Ngal are increasingly reported.[12,28]

Induction of mesenchymal–epithelial transition by Ngal is associated with upregulation of epithelial marker E-cadherin expression, but this is a slow process. In metanephric mesenchyme, morphologically distinct epithelia is observed only 7–10 days after addition of Ngal–siderophore–iron complex (unpublished observation).[15] By contrast, epithelia induced by leukemia-inhibitory factor can be observed within 4–5 days.[13,14] In Ras-transformed mammary cells, E-cadherin protein accumulation was evaluated 48 h after treatment with the complex.[30] Hanai *et al.*[30] demonstrated that treatment with Ngal–siderophore–iron suppresses Raf, mitogen-activated protein kinase (MEK)-1/2, extracellular signal-regulated kinase (ERK)-1/2 pathway of mitogen-activated protein kinase and inhibits E-cadherin phosphorylation, causing decrease in E-cadherin degradation. Not only treatment with Ngal–siderophore–iron complex but also transfection with cDNA and infection with adenovirus encoding Ngal results in mesenchymal–epithelial transition of transformed cells, implying that fetal calf serum or cells themselves provide mammalian siderophores. In the case of renal ischemia-reperfusion injury, phosphorylation of MEK1/2 and ERK1/2 is biphasic (transient activation within 30 min, followed by long-term activation for several days) and the levels of their phosphorylation are not necessarily parallel with the severity of renal injury,[35] suggesting that suppression of this pathway is not the major mechanism for Ngal-mediated kidney protection. Administration of Ngal is ineffective if given 2 h after reperfusion,[9] implying that Ngal is preventing the early injuries (in part by upregulating a protective enzyme heme oxygenase-1)[9] rather than stimulating the recovery process.

In healthy adult kidneys, Ngal[36] and other lipocalins (whose sizes are 17–43 kDa) including retinol-binding protein 4, α1-microglobulin[37] and probably also liver-type fatty acid-binding protein 1 and prostaglandin D synthase are freely filtrated in the glomeruli, bound to multiligand scavenger-receptor megalin (expressed abundantly and specifically on the brush borders of proximal tubules) and taken up efficiently by endocytosis (as well as albumin and β2-microglobulin).[38] Insufficient tubular reabsorption (owing to specific saturation in the endocytic pathway or general malfunctioning of proximal tubules) should contribute in part to urinary Ngal. Devireddy *et al.*[32] identified brain-type organic cation transporter as Ngal receptor in pro-B cells.

Iron-free siderophore-like activity (which assists the binding of Ngal and Fe^{3+}) is detectable in the normal urine of humans, mice, rats, and dogs.[9,39] Tear lipocalin, a major protein component specifically found in human tears, also binds with siderophores.[40] Lipocalin 12, found specifically in mouse epididymis, is also structurally related to Ngal and may have binding capacity for siderophores.[41]

CHARACTERISTICS OF NGAL AS RENAL FAILURE BIOMARKER

Ngal induction is a rapid event detectable within a few hours, characterizing Ngal as one of immediate early genes or acute-phase reactants such as IL-6 and C-reactive protein. Fold induction of Ngal mRNA and protein is log order of magnitude, reaching 1000-fold in most severe cases of renal injury.[9,39] Therefore, normalization for urinary creatinine level is not necessary to evaluate urinary Ngal.[21] Indeed, a patient with urinary Ngal level of 40 μg/ml died of multi-organ failure 12 h after urine collection[9] (Mori K *et al.*, unpublished observation).

DIRECTIONS FOR FUTURE RESEARCH

There are a number of siderohpre-dependent and -independent activities reported for Ngal. The role of endogenously expressed Ngal in these activities should be better verified using Ngal-deficient mice. During renal ischemia-reperfusion injury, the liver also starts to express Ngal mRNA.[39] Therefore, the source of Ngal protein in the blood and urine during renal injury can be a complex from the kidney, liver, and white blood cells (in the injured tissues and in circulation). Tissue-specific disruption of Ngal gene will make it possible to investigate what is the predominant source of Ngal, as a biomarker or as a protective mechanism for renal failure. Purification and identification of mammalian siderophores and to learn their metabolism and regulation are also important steps. The reported method to recognize siderophores is only available for iron-free molecules.[9] A new way to detect iron-loaded siderophores must be invented. Characterization of Ngal receptors, their downstream intracellular signaling, and subcellular localization of events will help elucidate the

detailed molecular mechanism underlying the actions of Ngal, siderophores, and iron.

CONCLUSION

Ngal is a very unique protein endowed with iron-carrying activity and diagnostic and therapeutic utilities for renal failure, which is acquiring an explosion of attention by researchers and clinicians beyond nephrology.

ACKNOWLEDGMENTS

Unfortunately, we could not describe all the contributors and original papers in Ngal research. We thank Drs. J Barasch, P Devarajan, and Q Al-awqati for discussion, instruction, and encouragement. We are also grateful to Drs. J Yang, KM Schmidt-Ott, JY Li, N Paragas, A Kalandadze, HT Lee, FH Cheema (Columbia University), and M Mukoyama, M Kasahara, H Yokoi, K Sawai, T Suganami, and T Kuwabara (Kyoto University). This work was supported by grants from Uehara Memorial Foundation, Yamanouchi Foundation for Research on Metabolic Disorders, Salt Science Research Foundation, Japanese Ministry of Education, Culture, Sports, Science and Technology, and from Japan Society for Promotion of Science.

REFERENCES

1. Flower DR, North AC, Sansom CE. The lipocalin protein family: structural and sequence overview. *Biochim Biophys Acta* 2000; **1482**: 9–24.
2. Yang Q, Graham TE, Mody N *et al.* Serum retinol binding protein 4 contributes to insulin resistance in obesity and type 2 diabetes. *Nature* 2005; **436**: 356–362.
3. Ragolia L, Palaia T, Hall CE *et al.* Accelerated glucose intolerance, nephropathy, and atherosclerosis in prostaglandin D2 synthase knockout mice. *J Biol Chem* 2005; **280**: 29946–29955.
4. Hotamisligil GS, Johnson RS, Distel RJ *et al.* Uncoupling of obesity from insulin resistance through a targeted mutation in aP2, the adipocyte fatty acid binding protein. *Science* 1996; **274**: 1377–1379.
5. Goetz DH, Holmes MA, Borregaard N *et al.* The neutrophil lipocalin NGAL is a bacteriostatic agent that interferes with siderophore-mediated iron acquisition. *Mol Cell* 2002; **10**: 1033–1043.
6. Raymond KN, Dertz EA, Kim SS. Enterobactin: an archetype for microbial iron transport. *Proc Natl Acad Sci USA* 2003; **100**: 3584–3588.
7. Barasch J, Mori K. Cell biology: iron thievery. *Nature* 2004; **432**: 811–813.
8. Takahashi M, Nakanishi H, Kawasaki S *et al.* Enhanced tolerance of rice to low iron availability in alkaline soils using barley nicotianamine aminotransferase genes. *Nat Biotechnol* 2001; **19**: 466–469.
9. Mori K, Lee HT, Rapoport D *et al.* Endocytic delivery of lipocalin-siderophore-iron complex rescues the kidney from ischemia-reperfusion injury. *J Clin Invest* 2005; **115**: 610–621.
10. Kjeldsen L, Johnsen AH, Sengelov H *et al.* Isolation and primary structure of NGAL, a novel protein associated with human neutrophil gelatinase. *J Biol Chem* 1993; **268**: 10425–10432.
11. Yan L, Borregaard N, Kjeldsen L *et al.* The high molecular weight urinary matrix metalloproteinase (MMP) activity is a complex of gelatinase B/MMP-9 and neutrophil gelatinase-associated lipocalin (NGAL). Modulation of MMP-9 activity by NGAL. *J Biol Chem* 2001; **276**: 37258–37265.
12. Gwira JA, Wei F, Ishibe S *et al.* Expression of neutrophil gelatinase-associated lipocalin regulates epithelial morphogenesis *in vitro*. *J Biol Chem* 2005; **280**: 7875–7882.
13. Mori K, Yang J, Barasch J. Ureteric bud controls multiple steps in the conversion of mesenchyme to epithelia. *Semin Cell Dev Biol* 2003; **14**: 209–216.
14. Barasch J, Yang J, Ware CB *et al.* Mesenchymal to epithelial conversion in rat metanephros is induced by LIF. *Cell* 1999; **99**: 377–386.
15. Yang J, Goetz D, Li JY *et al.* An iron delivery pathway mediated by a lipocalin. *Mol Cell* 2002; **10**: 1045–1056.
16. Flo TH, Smith KD, Sato S *et al.* Lipocalin 2 mediates an innate immune response to bacterial infection by sequestrating iron. *Nature* 2004; **432**: 917–921.
17. Li JY, Ram G, Gast K *et al.* Detection of intracellular iron by its regulatory effect. *Am J Physiol Cell Physiol* 2004; **287**: C1547–C1559.
18. Devarajan P. Update on mechanisms of ischemic acute kidney injury. *J Am Soc Nephrol* 2006; **17**: 1503–1520.
19. Supavekin S, Zhang W, Kucherlapati R *et al.* Differential gene expression following early renal ischemia/reperfusion. *Kidney Int* 2003; **63**: 1714–1724.
20. Mishra J, Ma Q, Prada A *et al.* Identification of neutrophil gelatinase-associated lipocalin as a novel early urinary biomarker for ischemic renal injury. *J Am Soc Nephrol* 2003; **14**: 2534–2543.
21. Mishra J, Dent C, Tarabishi R *et al.* Neutrophil gelatinase-associated lipocalin (NGAL) as a biomarker for acute renal injury after cardiac surgery. *Lancet* 2005; **365**: 1231–1238.
22. Wagener G, Jan M, Kim M *et al.* Association between increases in urinary neutrophil gelatinase-associated lipocalin and acute renal dysfunction after adult cardiac surgery. *Anesthesiology* 2006; **105**: 485–491.
23. Mishra J, Mori K, Ma Q *et al.* Amelioration of ischemic acute renal injury by neutrophil gelatinase-associated lipocalin. *J Am Soc Nephrol* 2004; **15**: 3073–3082.
24. Berger T, Togawa A, Duncan GS *et al.* Lipocalin 2-deficient mice exhibit increased sensitivity to Escherichia coli infection but not to ischemia-reperfusion injury. *Proc Natl Acad Sci USA* 2006; **103**: 1834–1839.
25. Cowland JB, Borregaard N. The individual regulation of granule protein mRNA levels during neutrophil maturation explains the heterogeneity of neutrophil granules. *J Leukoc Biol* 1999; **66**: 989–995.
26. Meheus LA, Fransen LM, Raymackers JG *et al.* Identification by microsequencing of lipopolysaccharide-induced proteins secreted by mouse macrophages. *J Immunol* 1993; **151**: 1535–1547.
27. Wang Y, Lam KS, Kraegen EW *et al.* Lipocalin-2 is an inflammatory marker closely associated with obesity, insulin resistance, and hyperglycemia in humans. *Clin Chem* 2007; **53**: 34–41.
28. Playford RJ, Belo A, Poulsom R *et al.* Effects of mouse and human lipocalin homologues 24p3/lcn2 and neutrophil gelatinase-associated lipocalin on gastrointestinal mucosal integrity and repair. *Gastroenterology* 2006; **131**: 809–817.
29. Cowland JB, Sorensen OE, Sehested M *et al.* Neutrophil gelatinase-associated lipocalin is up-regulated in human epithelial cells by IL-1 beta, but not by TNF-alpha. *J Immunol* 2003; **171**: 6630–6639.
30. Hanai J, Mammoto T, Seth P *et al.* Lipocalin 2 diminishes invasiveness and metastasis of Ras-transformed cells. *J Biol Chem* 2005; **280**: 13641–13647.
31. Liu Q, Nilsen-Hamilton M. Identification of a new acute phase protein. *J Biol Chem* 1995; **270**: 22565–22570.
32. Devireddy LR, Gazin C, Zhu X *et al.* A cell-surface receptor for lipocalin 24p3 selectively mediates apoptosis and iron uptake. *Cell* 2005; **123**: 1293–1305.
33. Devireddy LR, Teodoro JG, Richard FA *et al.* Induction of apoptosis by a secreted lipocalin that is transcriptionally regulated by IL-3 deprivation. *Science* 2001; **293**: 829–834.
34. Miharada K, Hiroyama T, Sudo K *et al.* Lipocalin 2 functions as a negative regulator of red lood cell production in an autocrine fashion. *FASEB J* 2005; **19**: 1881–1883.
35. Park KM, Kramers C, Vayssier-Taussat M *et al.* Prevention of kidney ischemia/reperfusion-induced functional injury MAPK and MAPK kinase activation, and inflammation by remote transient ureteral obstruction. *J Biol Chem* 2002; **277**: 2040–2049.
36. Hvidberg V, Jacobsen C, Strong RK *et al.* The endocytic receptor megalin binds the iron transporting neutrophil-gelatinase-associated lipocalin with high affinity and mediates its cellular uptake. *FEBS Lett* 2005; **579**: 773–777.
37. Leheste JR, Rolinski B, Vorum H *et al.* Megalin knockout mice as an animal model of low molecular weight proteinuria. *Am J Pathol* 1999; **155**: 1361–1370.
38. Moestrup SK, Verroust PJ. Megalin- and cubilin-mediated endocytosis of protein-bound vitamins, lipids, and hormones in polarized epithelia. *Annu Rev Nutr* 2001; **21**: 407–428.
39. Schmidt-Ott KM, Mori K, Kalandadze A *et al.* Neutrophil gelatinase-associated lipocalin-mediated iron traffic in kidney epithelia. *Curr Opin Nephrol Hypertens* 2006; **15**: 442–449.
40. Fluckinger M, Haas H, Merschak P *et al.* Human tear lipocalin exhibits antimicrobial activity by scavenging microbial siderophores. *Antimicrob Agents Chemother* 2004; **48**: 3367–3372.
41. Holmes MA, Paulsene W, Jide X *et al.* Siderocalin (Lcn 2) also binds carboxymycobactins, potentially defending against mycobacterial infections through iron sequestration. *Structure* 2005; **13**: 29–41.

THE JOURNAL OF BIOLOGICAL CHEMISTRY VOL. 282, NO. 40, pp. 29574–29583, October 5, 2007

Genetic and Pharmacological Inhibition of Rho-associated Kinase II Enhances Adipogenesis*

Received for publication, July 20, 2007 Published, JBC Papers in Press, August 6, 2007, DOI 10.1074/jbc.M705972200

Michio Noguchi‡, Kiminori Hosoda‡[1], Junji Fujikura‡, Muneya Fujimoto‡, Hiroshi Iwakura‡, Tsutomu Tomita‡, Takako Ishii‡, Naoki Arai‡, Masakazu Hirata‡, Ken Ebihara‡, Hiroaki Masuzaki‡, Hiroshi Itoh‡, Shuh Narumiya§, and Kazuwa Nakao‡

From the ‡Department of Medicine and Clinical Science, Kyoto University Graduate School of Medicine, Kyoto 606-8507, Japan and the §Department of Pharmacology, Kyoto University Faculty of Medicine, Kyoto 606-8501, Japan

Rho-associated kinase (ROCK) regulates reorganization of actin cytoskeleton. During adipogenesis, the structure of filamentous actin is converted from long stress fibers to cortical actin, suggesting that the ROCK is involved in adipogenesis. Two ROCK isoforms have been identified: ROCK-I and ROCK-II. However, pharmacological inhibitors of ROCK cannot distinguish two ROCK isoforms. In the present study, we examined the role of ROCK in adipogenesis and actin cytoskeleton using genetic and pharmacological approaches. Y-27632, which inhibits the activity of both ROCK isoforms, enhanced adipogenesis through the up-regulation of adipogenic transcription factors in 3T3-L1 cells. Furthermore, Y-27632 restored inhibition of adipogenesis by lysophosphatidic acid, which activates Rho. Regarding actin cytoskeleton, Y-27632 disrupted stress fibers in 3T3-L1 preadipocytes. Next, we analyzed adipogenesis of mouse embryonic fibroblasts (MEFs) derived from ROCK-I and ROCK-II knock-out mice, respectively. Adipogenesis of ROCK-II (−/−) MEFs was markedly enhanced compared with wild-type MEFs while that of ROCK-I (−/−) MEFs was not. In contrast to pharmacological approaches, no obvious alteration was found in actin cytoskeleton of ROCK-II (−/−) MEFs compared with wild-type MEFs. In 3T3-L1 cells, knockdown of ROCK-II by RNA interference enhanced the expression of adipogenic transcription factors while that of ROCK-I did not. Moreover, Y-27632 inhibited IRS-1 serine phosphorylation and enhanced Akt phosphorylation in 3T3-L1 preadipocytes. Similarly, Akt phosphorylation in ROCK-II (−/−) MEFs was augmented compared with wild-type MEFs. In conclusion, inhibition of ROCK-II, not ROCK-I, enhances adipogenesis accompanied by the up-regulation of adipogenic transcription factors. Augmentation of insulin signaling may contribute to the enhancement of adipogenesis.

Adipogenesis is an area of intense interest because of the large and growing prevalence of obesity, insulin resistance, and type 2 diabetes (1, 2). Studies with *in vitro* models, such as 3T3-L1 and 3T3-F442A cell lines, have clarified the mechanisms of adipogenesis (3, 4). In 3T3-L1 cells, adipocyte differentiation is a process regulated by multiple transcription factors, principally the CCAAT/enhancer-binding protein (C/EBP)[2] family and peroxisome proliferator-activated receptor γ (PPARγ). In the presence of hormonal inducers, the expression of C/EBPβ and C/EBPδ temporarily increases (5), followed by the expression of PPARγ and C/EBPα (6, 7). A cooperative interaction between PPARγ and C/EBPα drives the expression of genes that are necessary for the generation and maintenance of the adipogenic phenotype such as lipid accumulation and insulin sensitivity (8).

During adipogenesis, adipocytes morphologically change from fibroblastic cells to round and lipid-laden cells. It is well known that actin cytoskeleton regulates the morphology of the cells (9). Concerning adipogenesis and actin cytoskeleton, it has been reported that adipocyte differentiation results in the conversion of filamentous actin (F-actin) from stress fibers and lamellipodia to cortical actin structures (10).

During the past several decades, many studies have shed light on the molecular mechanisms of actin cytoskeletal regulation. Members of the Rho family are essential regulatory components of the signaling pathway that directs reorganization of actin cytoskeleton. Small GTPase Rho contributes to many cellular functions such as cell motility, adhesion, and cytokinesis through reorganization of actin cytoskeleton. Rho is activated by extracellular signals such as lysophosphatidic acid (LPA). The actions of Rho are mediated by downstream Rho effectors. One of these effectors is Rho-associated kinase (ROCK) (11, 12). Two ROCK isoforms have been identified: ROCK-I (also known as ROKβ) and ROCK-II (also known as Rho kinase and ROKα) (13–16). ROCK mediates Rho signaling and reorganizes actin cytoskeleton through phosphorylation of several substrates that contribute to the assembly of actin filaments and contractility. Elucidation of the role of ROCK has been facilitated by the introduction of ROCK inhibitors, Y-27632 and fasudil. Studies with these inhibitors have revealed that ROCK

* This work was supported by research grants from the Japanese Ministry of Education, Culture, Sports, Science, and Technology and the Japanese Ministry of Health, Labor and Welfare. This work was also supported in part by a grant from the Smoking Research Foundation. The costs of publication of this article were defrayed in part by the payment of page charges. This article must therefore be hereby marked "*advertisement*" in accordance with 18 U.S.C. Section 1734 solely to indicate this fact.

[1] To whom correspondence should be addressed: Dept. of Medicine and Clinical Science, Kyoto University Graduate School of Medicine, 54 Shogoin Kawahara-cho, Sakyo-ku, Kyoto 606-8507, Japan. Tel.: 81-75-751-3172; Fax: 81-75-771-9452; E-mail: kh@kuhp.kyoto-u.ac.jp.

[2] The abbreviations used are: C/EBP, CCAAT/enhancer-binding protein; IRS, insulin receptor substrate; ERK, extracellular signal-related kinase; MAPK, mitogen-activated protein kinase; CS, calf serum; FBS, fetal bovine serum; DMEM, Dulbecco's modified Eagle medium; BSA, bovine serum albumin; PI3K, phosphatidylinositol 3-kinase; IGF-1, insulin-like growth factor-1; ROCK, Rho-associated kinase; PPARγ, proliferator-activated receptor γ; LPA, lysophosphatidic acid.

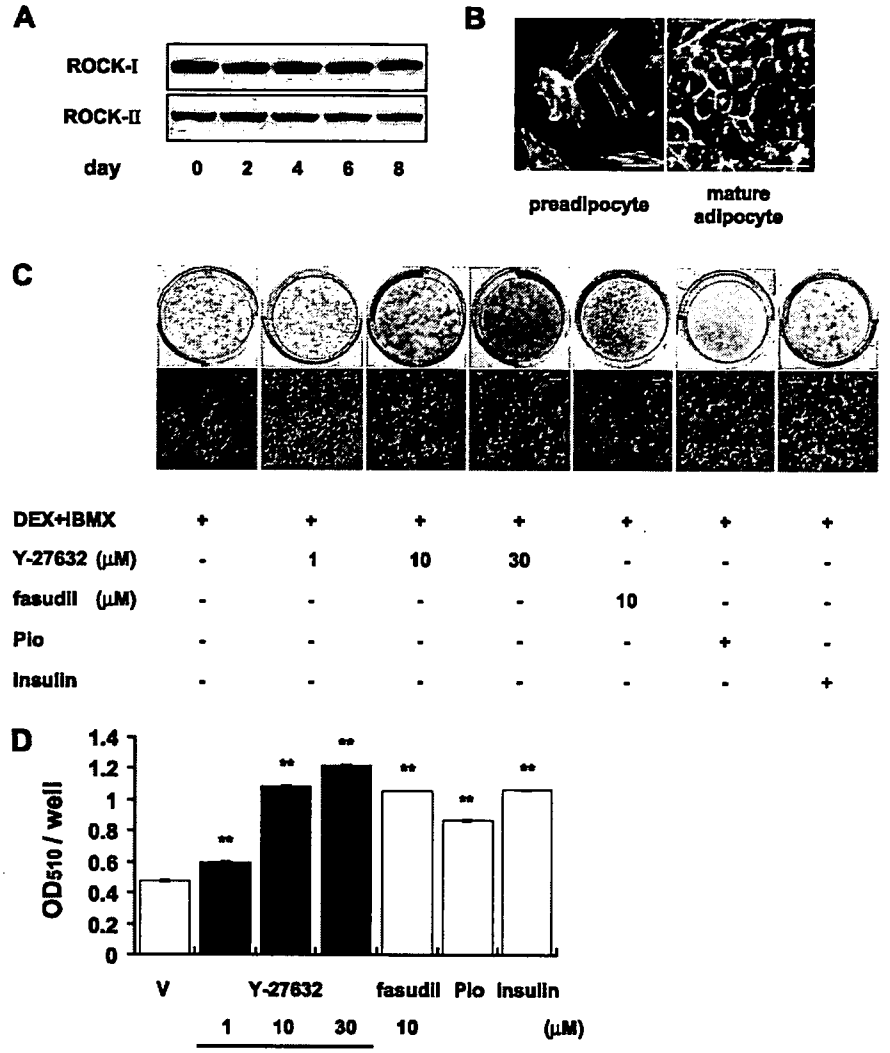

FIGURE 1. **ROCK expression and actin cytoskeleton during adipogenesis and effect of ROCK inhibitors on adipogenesis.** *A*, equal amounts of proteins harvested from day 0 to day 8 were subjected to Western blot analysis using antibodies against ROCK-I and ROCK-II. *B*, 3T3-L1 preadipocytes and mature adipocytes were fixed, permeabilized, and stained with Oregon Green phalloidin for F-actin. *Bar*, 50 μm. *C*, differentiated adipocytes were fixed and stained with Oil Red O at day 8. Macroscopic and microscopic pictures of cells are shown. *D*, lipid accumulation was assessed by the quantification of A_{510} in destained Oil Red O with isopropyl alcohol. Data are expressed as mean ± S.E. from triplicate experiments. **, $p < 0.01$ (Student's *t* test) compared with dexamethasone and IBMX-treated group. *Pio*, pioglitazone, *V*, vehicle.

regulates various physiological and pathological processes (17–20), while they cannot refer to the isoform-specific role of ROCK because ROCK inhibitors inhibit the activity of both ROCK-I and ROCK-II. Furthermore, ROCK inhibitors may potentially inhibit other protein kinases such as protein kinase A (12).

Several studies have reported that Rho-ROCK pathway is involved in adipogenesis (21, 22). However, the role of ROCK in adipogenesis still remains to be clarified. We show here the effects of inhibition of ROCK on adipogenesis and examine the molecular mechanisms using pharmacological and genetic approaches. Especially, the adipogenic analysis using MEFs derived from ROCK-I or ROCK-II knock-out mice and ROCK-I or ROCK-II siRNA can provide the evidence about the physiological role of ROCK and the isoform-specific role of ROCK in adipogenesis.

EXPERIMENTAL PROCEDURES

Materials—Y-27632 and pioglitazone (AD-4833) were provided by Mitsubishi Pharma (Osaka, Japan) and Takeda Pharmaceutical Company (Osaka, Japan), respectively. Insulin was purchased from Roche Applied Science (Mannheim, Germany). 3-Isobutyl-1-methylxanthine (IBMX) and dexamethasone were purchased from Nacalai Tesque, Inc. (Kyoto, Japan). LPA and wortmannin were obtained from Sigma-Aldrich (Tokyo, Japan). Fasudil was obtained from Calbiochem. Polyclonal antibodies against ROCK-I, ROCK-II, C/EBPα, C/EBPδ, PPARγ, and IRS-1 were purchased from Santa Cruz Biotechnology (Santa Cruz, CA). Monoclonal antibodies against C/EBPβ and adiponectin were obtained from Affinity BioReagents (Golden, CO). The monoclonal antibody against aP2 was purchased from R&D Systems (Minneapolis, MN). Polyclonal antibodies against Akt, phospho-Akt (Ser^{473}), phospho-IRS-1 ($Ser^{632/635}$), phospho-IRS-1 (Ser^{612}), ERK1/2, phospho-ERK1/2, p38MAPK, and phospho-p38MAPK were purchased from Cell Signaling Technology Inc. (Beverly, MA). Horseradish peroxidase-conjugated anti-mouse, anti-rat, and anti-rabbit IgG antibodies and ECL plus Western detecting kit were purchased from Amersham Biosciences.

Cell Culture, Adipocyte Differentiation, and Oil Red O Staining—3T3-L1 cells (kindly provided by Dr. H. Green and Dr. M. Morikawa, Harvard Medical School, Boston, MA) were cultured and differentiated into adipocytes as described previously (23). Briefly, cells were grown for 2 days post-confluence (referred as day 0) in 10% CS/DMEM. Differentiation was induced with 10% FBS/DMEM containing 0.5 mM IBMX, 0.25 μM dexamethasone, and 1 μg/ml insulin for 2 days. The cells were then incubated in 10% FBS/DMEM with insulin for 2 days and maintained hereafter with 10% FBS/DMEM to day 8. Pioglitazone was dissolved in Me_2SO and added to media within 0.1% of volume. The medium was changed every other day. At day 8, the cells were washed with phosphate-buffered saline (PBS) twice, fixed in 3.7% formaldehyde for 1 h and then stained with 0.6% (w/v) Oil Red O solution (60% isopropyl alcohol, 40% water) for 2 h at room temperature. Cells were then

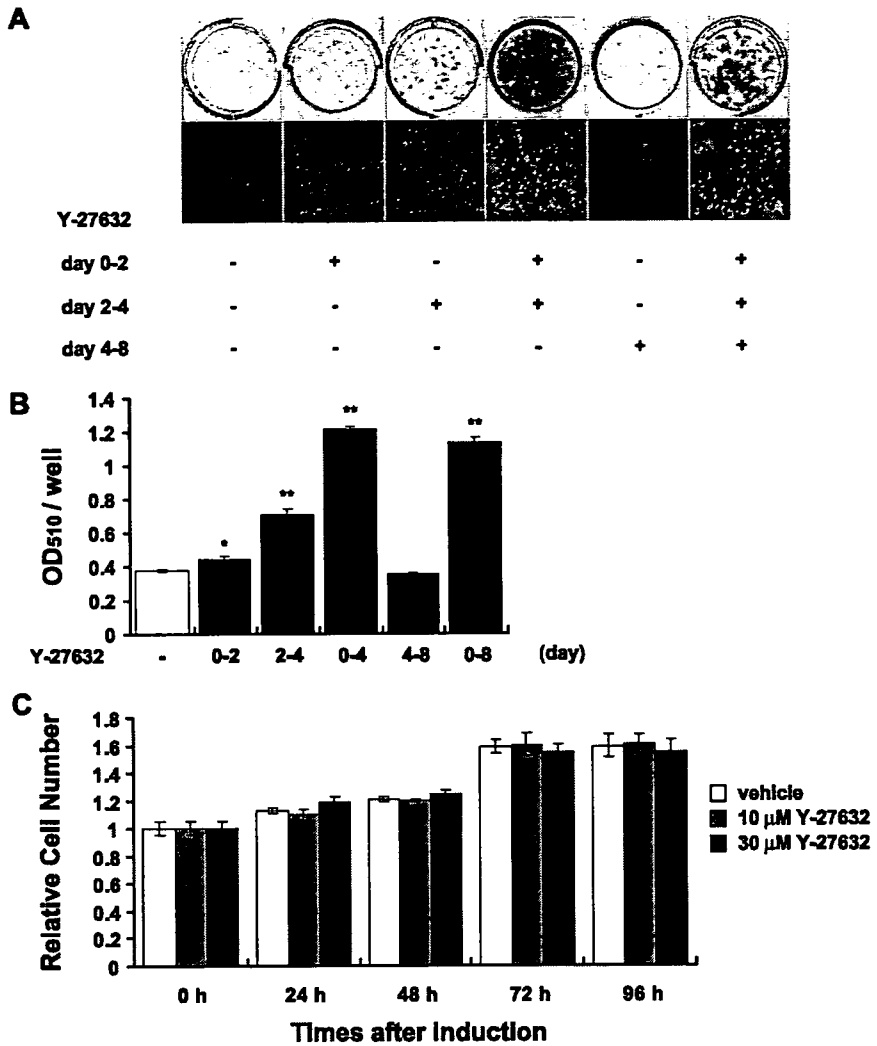

FIGURE 2. **Effect of Y-27632 during 3T3-L1 adipogenesis.** *A*, in the presence of dexamethasone and IBMX, 30 μM Y-27632 was supplemented from day 0 to day 2, day 2 to day 4, day 0 to day 4, day 4 to day 8 or day 0 to day 8, respectively. Differentiated adipocytes were fixed and stained with Oil Red O at day 8. Macroscopic and microscopic pictures of cells are shown. *B*, lipid accumulation was assessed by the quantification of A_{510} in destained Oil Red O with isopropyl alcohol. Data are expressed as mean ± S.E. from triplicate experiments. *, $p < 0.05$ (Student's *t* test) compared with dexamethasone and IBMX-treated group. **, $p < 0.01$ (Student's *t* test) compared with dexamethasone and IBMX-treated group. *C*, relative cell number during adipogenesis. 10 μM or 30 μM Y-27632 was added from day 0 to day 4 in the presence of dexamethasone and IBMX. Proliferation of MEFs was assessed by counting cells at the indicated times. Data are expressed as mean ± S.E. from triplicate experiments.

washed with water to remove unbound dye. Stained Oil Red O was eluted with isopropyl alcohol and quantified by measuring the optical absorbance at 510 nm (24).

Preparation of Primary Mouse Embryonic Fibroblasts and Induction of Adipogenesis—The generation of ROCK-I and ROCK-II knock-out mice was previously reported (25, 26). ROCK-II knock-out mice of a mixed background 129/Sv and C57BL/6N genetic background were backcrossed to the C57BL/6N strain for more than 8 generations. Primary MEFs were harvested from 13.5 d.p.c. embryos of each genotype as previously described (27). Differentiation of MEFs was induced with 0.5 mM IBMX, 0.25 μM dexamethasone and 10 μg/ml insulin for 6 days and maintained with 10% FBS/DMEM to day 8.

Small Interfering RNA (siRNA)—Synthetic siRNAs were purchased from Invitrogen (Carlsbad, CA). siRNAs were delivered into 3T3-L1 cells by a pulse of electroporation with Nucleofector (Amaxa, Gaithersburg, MD). After the electroporation, cells were immediately mixed with the fresh medium for 10 min and reseeded on plates for further examinations. The cells were differentiated 12 h after the electroporation. Negative control siRNA was used as the control of experiments. The targeted nucleotide sequences of the siRNAs were ATTGGTGCTTGTCAGTTAGGCGTGC (ROCK-I) and ATAATTACTCATAAGGTTGACGAGG (ROCK-II).

Preparation of Total Cell Lysates and Western Blot Analysis—Cells were washed twice with ice-cold PBS and harvested in a lysis buffer (40 mM HEPES, 10 mM EDTA, 100 mM NaF, 10 mM sodium pyrophosphate, 1 mM Na_3VO_4, 50 μM okadaic acid, 1% (v/v) Nonidet P-40, 1 mM phenylmethylsulfonyl fluoride, and 0.1 mg/ml aprotinin at pH 7.5). For the examination of transcription factors, cells were harvested in a lysis buffer (60 mM Tris-HCl and 1% SDS at pH 6.8). Lysates were heated at 100 °C for 10 min. After centrifugation, supernatants were normalized for protein concentration via the Bradford method and subjected to immunoblotting. For Western blot analysis, proteins were subjected to SDS-PAGE and electroblotted to polyvinylidene fluoride membranes (Polyscreen, NEN Life Science Products, Inc., Boston, MA). Transferred membranes were blocked with Block Ace (Yukijirushi Nyugyo, Sapporo, Japan) and then incubated with the primary antibodies. After washing with PBS, membranes were reacted with secondary antibodies and developed with ECL plus as instructed by the manufacturer. The signal on the blot was detected and quantified with Lumino-Image Analyser LAS-1000 System (Fuji Photo Film Co., Tokyo, Japan).

Immunofluorescence Study—The cells were washed once with PBS and fixed as follows. 3T3-L1 cells were fixed first for 1 min with 4% formaldehyde and 0.1% Triton X in PBS and then for 15 min with 4% formaldehyde alone in PBS. The cells were permeabilized by washing in PBS containing 0.1% Triton X for 5 min and incubated with PBS containing 3% bovine serum albumin for 60 min at room temperature. F-actin was stained with Oregon Green phalloidin (Molecular Probes, Carlsbad, CA). Optical sections were obtained with a Carl Zeiss LSM5 Pascal.

Quantitative Real-time PCR—Total RNA was prepared using TRIzol Reagent (Invitrogen). For quantitative RT-PCR assay, cDNA was synthesized by iScript (Bio-Rad). To determine ROCK-I, ROCK-II, PPARγ, and C/EBPα mRNA levels, these probes and primers were employed. ROCK-I-specific primers, sense: 5′-AGGAAAATACAGGAACTGCAAAGTG-3′, antisense: 5′-CTTTCTTGCTTTCCTGAGTCAACTC-3′ and probe: 5′-GTCTTCCAGAATCCCTCGCGCCAGCT-3′; ROCK-II-specific primers, sense: 5′-AAGACAGCGACATT-GAACAGC-3′, antisense: 5′-ACCATCCTTCTAATCTTGA-TTCTGG-3′ and probe: 5′-GATCCATCAGGCTCAGCATC-GCC-3′; PPARγ-specific primers, sense: 5′-CCCAGAGCAT-GGTGCCTT-3′, antisense: 5′-GGCATCTCTGTGTCAACC-ATGGT-3′ and probe: 5′-CTGATGCACTGCCTATGAGCA-CTTCACA-3′; C/EBPα-specific primers, sense: 5′-CGCCTT-CAACGACGAGTTC-3′, antisense: 5′-TTGGCCTTCTCCT-GCTGTC-3′, and probe: 5′-TGGCCGACCTCTTCCAGC-ACAG-3′. TaqMan PCR was performed using ABI Prism 7300 Sequence Detection System as instructed by manufacturer (Applied Biosystems, Foster City, CA). Levels of mRNA were normalized to those of 18S mRNA.

Statistical Analysis—Data are presented as means ± S.E. Student's *t* test was used to compare with the control. Differences were accepted as significant at $p < 0.05$ level.

RESULTS

ROCK Expression and Actin Cytoskeleton during Adipogenesis and Effect of ROCK Inhibitors on Adipogenesis—We detected protein expression of ROCK in 3T3-L1 cells by Western blot analysis (Fig. 1*A*). In 3T3-L1 preadipocytes (day 0) and mature adipocytes (day 8), both ROCK-I and ROCK-II were expressed. The expression levels of two ROCK isoforms did not significantly change during adipogenesis. Then, we observed actin cytoskeleton by phalloidin staining at preadipocytes and mature adipocytes. During adipogenesis, the structure of filamentous actin was converted from long stress fiber (preadipocyte) to cortical actin (mature adipocyte), suggesting that Rho-ROCK pathway is involved in adipogenesis (Fig. 1*B*). To examine the effects of ROCK inhibitors on adipogenesis, 3T3-L1 cells were exposed to 1 μM, 10 μM, 30 μM Y-27632, 10 μM fasudil, 1 μM pioglitazone, and 1 μg/ml insulin, respectively in the presence of dexamethasone and IBMX. Y-27632, fasudil, or pioglitazone was added to media from day 0 to day 8. Insulin was added to media from the start of differentiation (day 0) to day 4. At day 8, we evaluated the lipid accumulation by Oil Red O staining (Fig. 1, *C* and *D*). Y-27632 enhanced lipid accumulation in a dose-dependent manner. Y-27632 or fasudil-treated dishes accumulated lipid droplets markedly compared with vehicle-treated dishes, indicating that ROCK inhibitors enhance adipogenesis. Consistent with previous reports (28–30), insulin and pioglitazone enhanced lipid accumulation, respectively. Then, to determine when the ROCK inhibitor principally affects adipogenesis, 30 μM Y-27632 was added in various periods of 3T3-L1 adipogenesis stimulated by dexamethasone and IBMX (Fig. 2, *A* and *B*). The exposure of 30 μM Y-27632 during days 0–4 fully enhanced lipid accumulation, while during days 4–8, Y-27632 did not enhance it at all. In cases of days 0–2 and 2–4, Y-27632 partially enhanced lipid accumulation. Treatment with 10 μM or 30 μM Y-27632 did not significantly alter total cell number during adipogenesis compared with vehicle treatment (Fig. 2*C*).

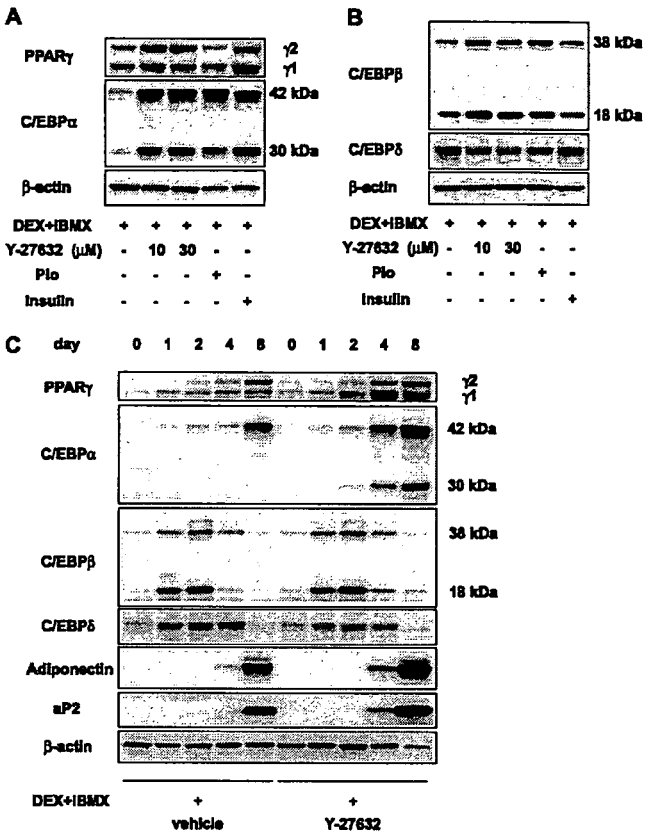

FIGURE 3. **Effect of Y-27632 on protein expression of adipogenic genes.** *A*, equal amounts of proteins harvested at day 4 were subjected to Western blot analysis using antibodies against PPARγ, C/EBPα, and β-actin. *B*, equal amounts of proteins harvested at day 2 were subjected to Western blot analysis using antibodies against C/EBPβ, C/EBPδ, and β-actin. *C*, equal amounts of proteins harvested at day 0, 1, 2, 4, and 8 were subjected to Western blot analysis using antibodies against PPARγ, C/EBPα, C/EBPβ, C/EBPδ, aP2, adiponectin, and β-actin. β-Actin proteins were monitored as hallmarks during adipocyte differentiation. *Pio*, pioglitazone. All data are representatives of at least three independent experiments.

Effect of Y-27632 on the Expression of Adipogenic Genes—Because ROCK inhibitors enhanced lipid accumulation, we examined the expression of adipogenic transcription factors C/EBPβ and C/EBPδ at day 2, and C/EBPα and PPARγ at day 4 by Western blot analysis (Fig. 3, *A* and *B*). In the presence of dexamethasone and IBMX, Y-27632 with a concentration of 30 μM augmented the expression of C/EBPβ (~1.8-fold increase), C/EBPα (~6.5-fold increase) and PPARγ (~5.6-fold increase) while it suppressed that of C/EBPδ (~40% decrease) compared with the non-treated group. 1 μg/ml insulin did not affect the expression of C/EBPβ and C/EBPδ at day 2 while it enhanced that of C/EBPα and PPARγ at day 4. 1 μM pioglitazone augmented the expression of C/EBPβ and C/EBPα while it suppressed those of C/EBPδ and PPARγ. The effects of insulin and pioglitazone on the expression of adipogenic trasnscription factors were compatible with previous reports (29, 31). Furthermore, we examined protein expression of adipogenic genes during the course of differentiation; day 0, day 1, day 2, day 4, and day 8 (Fig. 3*C*). Compared with the vehicle treatment

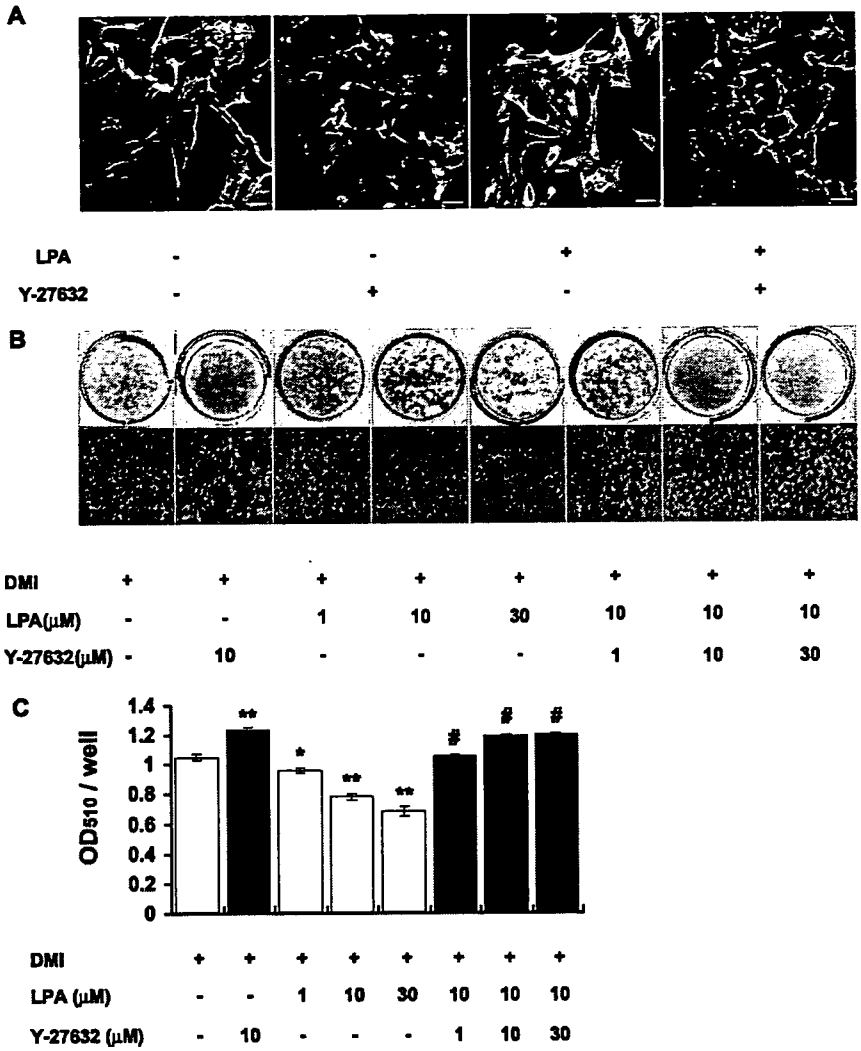

FIGURE 4. **Effect of LPA and Y-27632 on actin cytoskeleton and adipogenesis of 3T3-L1 preadipocytes.** *A*, 3T3-L1 cells were treated or not treated with 30 μM Y-27632 for 2 h, then exposed to 10 μM LPA for 0 and 5 min. The cells were fixed, permeabilized, and stained with Oregon Green phalloidin for F-actin. *Bar*, 50 μm. *B*, differentiated adipocytes were fixed and stained with Oil Red O at day 8. Macroscopic and microscopic pictures of cells are shown. *C*, lipid accumulation was assessed by the quantification of A_{510} in destained Oil Red O with isopropyl alcohol. Data are expressed as mean ± S.E. from triplicate experiments. *, $p < 0.05$ (Student's *t* test) compared with DMI-treated group. **, $p < 0.01$ (Student's *t* test) compared with DMI-treated group. #, $p < 0.01$ (Student's *t* test) compared with 10 μM LPA-treated group. DMI, dexamethasone, IBMX, and insulin.

group, 30 μM Y-27632 enhanced the expression of adipogenic transcription factors: C/EBPβ (~1.7-fold increase, day 1), PPARγ (~5.2-fold increase, day 4), and C/EBPα (~11.7-fold increase, day 4) and adipogenic late markers: aP2 (~8.9-fold increase, day 4) and adiponectin (~8.1-fold increase, day 4). Also in this analysis, Y-27632 suppressed the expression of C/EBPδ (~31% decrease, day 2).

Effect of LPA and Y-27632 on Actin Cytoskeleton and Adipogenesis—LPA activates small GTPase Rho via specific G protein-coupled receptors: LPA_{1-4} (32). It has been reported that LPA induces the stress fiber formation in Swiss 3T3 fibroblast, which is inhibited by Y-27632 (33, 34). Therefore, we examined the regulation of actin cytoskeleton by LPA and Y-27632 in 3T3-L1 preadipocytes (Fig. 4*A*). We stimulated serum-starved 3T3-L1 preadipocytes with or without 10 μM LPA after the pretreatment of 30 μM Y-27632 or non-treatment and assessed the effects on actin cytoskeleton by staining cells with phalloidin. LPA addition to serum-starved 3T3-L1 cells spread the cells and induced stress fibers while this change was inhibited by Y-27632. In Y-27632-treated cells without LPA addition, we could not observe stress fibers or thick actin rim in the cell periphery.

We examined the effects of Y-27632 on LPA-treated 3T3-L1 cells by Oil Red O staining. LPA and Y-27632 were added to media from day 0 to day 8. In the presence of dexamethasone, IBMX, and insulin, 10 μM Y-27632 enhanced adipogenesis (~20% increase) while 30 μM LPA inhibited it (~32% decrease), consistent with a previous report in 3T3-F442A cells (32). In 3T3-L1 cells, LPA inhibited adipogenesis in a dose-dependent manner with concentrations of 1 μM, 10 μM, and 30 μM. Y-27632 completely restored its inhibition with concentrations of 10 μM and 30 μM (Fig. 4, *B* and *C*).

Adipogenesis of ROCK-II (−/−) and ROCK-I (−/−) MEFs—To establish more directly causal link between ROCK and adipogenesis, primary mouse embryonic fibroblasts (MEFs) prepared from ROCK-II (+/+), ROCK-II (+/−), ROCK-II (−/−), and ROCK-I (+/+), ROCK-I (+/−), ROCK-I (−/−) mice were subjected to the adipogenic induction culture. Disruption of ROCK-I and ROCK-II protein was confirmed by Western blot analysis (Figs. 5*B* and 6*B*). ROCK-II protein levels in ROCK-I (+/+), ROCK-I (+/−), and ROCK-I (−/−) mice did not differ between genotypes. Similarly, ROCK-I protein levels in ROCK-II (+/+), (+/−), and (−/−) mice did not differ between genotypes. These results show that there is no compensatory increase in expression of the other ROCK isoform. After adipogenic induction, we examined lipid accumulation by Oil Red O staining and the expression of adipogenic transcription factors by Taqman PCR at day 8. ROCK-II (−/−) MEFs exhibited the enhancement of lipid accumulation compared with wild-type MEFs and mRNA levels of PPARγ and C/EBPα were markedly enhanced compared with wild-type MEFs (~14.2-fold and ~6.2-fold increase, respectively; **, $p < 0.01$). ROCK-II (+/−) MEFs also exhibited the enhancement of lipid accumulation compared with wild-type MEFs and mRNA levels of PPARγ and C/EBPα were significantly enhanced compared with wild-type MEFs (~5.4-fold and ~4.4-fold increase, respectively;

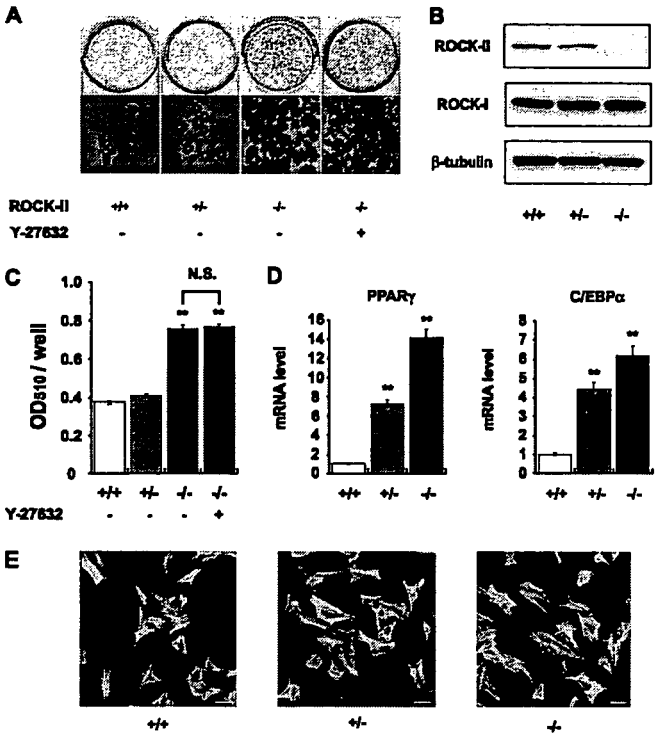

FIGURE 5. **Adipogenesis of ROCK-II (−/−) MEFs.** *A*, differentiated MEFs were fixed and stained with Oil Red O at day 8. Macroscopic and microscopic pictures of cells are shown. 30 μM Y-27632 was supplemented in the differentiation medium of ROCK-II (−/−) MEFs. *B*, equal amounts of proteins were subjected to Western blot analysis using antibodies against ROCK-I, ROCK-II, and β-tubulin. *C*, lipid accumulation was assessed by the quantification of A_{510} in destained Oil Red O with isopropyl alcohol. Data are expressed as mean ± S.E. from triplicate experiments. **, $p < 0.01$ (Student's *t* test) compared with ROCK-II (+/+) MEFs. *D*, expression of mRNA for PPARγ and C/EBPα from ROCK-II (+/+), (+/−) and (−/−) MEFs. Data are expressed as mean ± S.E. **, $p < 0.01$ (Student's *t* test) compared with ROCK-II (+/+) MEFs. $n = 6$ in each group. *E*, actin cytoskeleton of MEFs. Before adipogenic induction, the cells were fixed, permeabilized, and stained with Oregon Green phalloidin for F-actin. *Bar*, 50 μm.

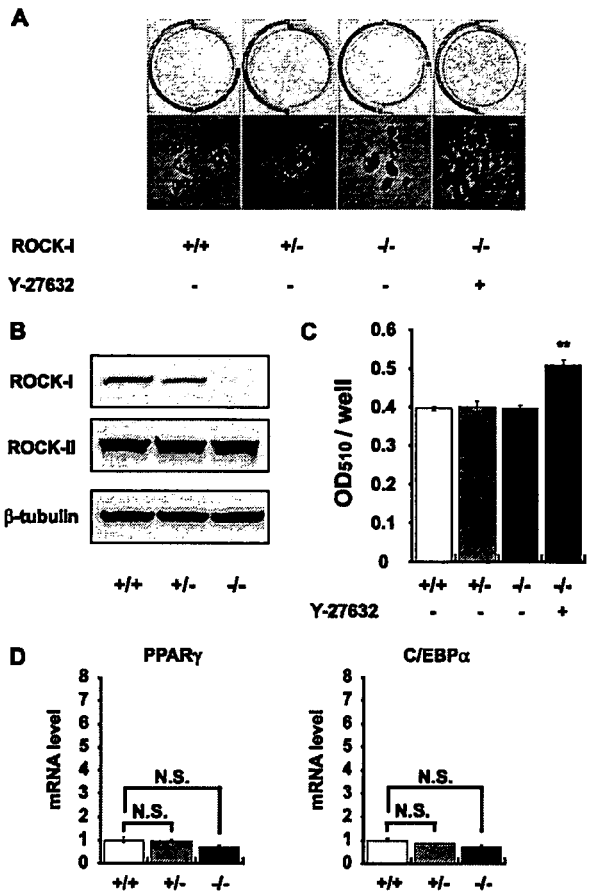

FIGURE 6. **Adipogenesis of ROCK-I (−/−) MEFs.** *A*, differentiated MEFs were fixed and stained with Oil Red O at day 8. Macroscopic and microscopic pictures of cells are shown. 30 μM Y-27632 was supplemented in the differentiation medium of ROCK-I (−/−) MEFs. *B*, equal amounts of proteins were subjected to Western blot analysis using antibodies against ROCK-I, ROCK-II, and β-tubulin. *C*, lipid accumulation was assessed by the quantification of A_{510} in destained Oil Red O with isopropyl alcohol. Data are expressed as mean ± S.E. from triplicate experiments. **, $p < 0.01$ (Student's *t* test) compared with ROCK-I (+/+) MEFs. *D*, expression of mRNA for PPARγ and C/EBPα from ROCK-I (+/+), (+/−), and (−/−) MEFs. Data are expressed as mean ± S.E. *N.S.*, not significant. $n = 6$ in each group.

**, $p < 0.01$). 30 μM Y-27632 did not enhance lipid accumulation in ROCK-II (−/−) MEFs, significantly (Fig. 5, *A*, *C*, and *D*). Before adipogenic induction, the architecture of actin cytoskeleton in ROCK-II (−/−) MEFs did not change compared with wild-type MEFs (Fig. 5*E*). The percentage of stress fiber positive cells was not significantly altered ((+/+), 96.67 ± 3.33%; (+/−), 97.22 ± 2.77%; (−/−), 97.1 ± 1.5%). In ROCK-I (−/−) MEFs, adipogenesis was not significantly enhanced compared with wild-type MEFs. Lipid accumulation and mRNA levels of PPARγ and C/EBPα did not differ between each genotype. Furthermore, 30 μM Y-27632 enhanced lipid accumulation in ROCK-I (−/−) MEFs (Fig. 6, *A*, *C*, and *D*).

Effect of Knockdown of ROCK on Expression of Adipogenic Transcription Factors—To determine whether inhibition of ROCK-II enhances adipogenesis in 3T3-L1 cells, we examined the effect of ROCK-I or ROCK-II knockdown on 3T3-L1 adipogenesis using siRNA technique. We introduced siRNA targeted for ROCK-I or ROCK-II into 3T3-L1 preadipocytes. 3T3-L1 cells were differentiated 12 h after introduction of siRNA. We confirmed the knockdown of ROCK-I or ROCK-II expression by Western blot analysis at day 2. Compared with the negative control group, introduction of ROCK-I and ROCK-II siRNA resulted in ~96 and ~86% decrease, respectively (Fig. 7, *A* and *B*). There was no obvious compensatory increase of the expression of the other ROCK isoform. At day 3, we examined the expression of adipogenic transcription factors by quantitative RT-PCR. ROCK-II siRNA enhanced the expression of PPARγ and C/EBPα compared with the control (~2.1-fold and ~1.8-fold increase, respectively, **, $p < 0.01$) (Fig. 7*C*). ROCK-I siRNA did not enhance the expression of PPARγ and C/EBPα significantly (Fig. 7*D*).

Effect of Inhibition of ROCK on Intracellular Signaling Pathway—We addressed the mechanisms of downstream signaling of Rho-ROCK. It is known that ROCK directly associates with IRS-1 and phosphorylates its serine residues (35–37). We stimulated serum-starved 3T3-L1 preadipocytes with insulin after the pretreatment of Y-27632. 30 μM Y-27632 inhibited insulin-induced IRS-1 Ser^{612} (~35% decrease, **, $p < 0.01$) and IRS-1 $Ser^{632/635}$ (~36% decrease, **, $p < 0.01$) phosphorylation and markedly enhanced insulin-induced Akt phosphorylation (~3.6-fold increase, **, $p < 0.01$) compared with non-treated

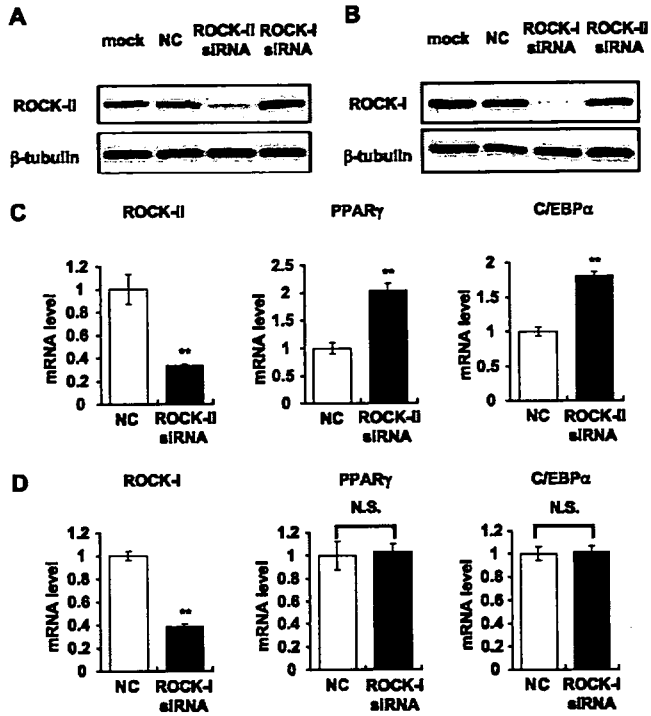

FIGURE 7. **Effect of knockdown of ROCK-I or ROCK-II on 3T3-L1 adipogenesis by RNA interference.** *A*, ROCK-II protein level was determined 48 h after adipogenic induction by Western blot analysis using antibodies against ROCK-II and β-tubulin. *B*, ROCK-I protein level was determined 48 h after adipogenic induction by Western blot analysis using antibodies against ROCK-I and β-tubulin. *C*, expression of mRNA for PPARγ, C/EBPα, and ROCK-II harvested at day 3. Data are expressed as mean ± S.E. **, $p < 0.01$ (Student's *t* test) compared with a negative control. $n = 6$ in each group. *D*, expression of mRNA for PPARγ, C/EBPα, and ROCK-I harvested at day 3. Data are expressed as mean ± S.E. *N.S.*, not significant. *NC*, negative control. $n = 6$ in each group.

groups (Fig. 8, *A* and *C*). Regarding MAPK signaling, Y-27632 slightly enhanced p38MAPK phosphorylation (~1.1-fold increase) and inhibited ERK1/2 phosphorylation (~23% decrease) upon the stimulation of insulin (Fig. 8*B*). We examined whether an inhibitor of PI3-kinase, wortmannin, blocks the enhancement of 3T3-L1 adipogenesis induced by Y-27632. Wortmannin and Y-27632 were added to media from day 0 to day 8. Wortmannin with concentrations of 100 nM and 1 μM inhibited the enhancement of preadipocyte differentiation induced by 10 μM Y-27632 in the presence of dexamethasone and IBMX (Fig. 8*D*). We examined insulin-induced Akt phosphorylation in ROCK-II knock-out MEFs. In ROCK-II (−/−) and (+/−) MEFs, insulin-induced Akt phosphorylation was significantly enhanced compared with wild-type MEFs (5 min after stimulation; ~6.0-fold increase and ~2.8-fold increase, respectively, **, $p < 0.01$) (Fig. 9*A*). In ROCK-I MEFs, there is no significant difference in insulin-induced Akt phosphorylation between each genotype (Fig. 9*B*).

DISCUSSION

In the present study, we show that inhibition of ROCK enhances adipogenesis. It is impossible to determine the isoform-specific role of ROCK by treatment of ROCK inhibitors. In addition to pharmacological approaches, we examined the adipogenesis of both ROCK-I (−/−) MEFs and ROCK-II (−/−) MEFs. Furthermore, we examined the effects of knockdown of ROCK-I or ROCK-II on 3T3-L1 adipogenesis by RNA interference. To the best of our knowledge, this is the first study demonstrating that inhibition of ROCK-II enhances adipogenesis and insulin-induced Akt phosphorylation. Our results suggest that ROCK-II plays an important role in adipogenesis and insulin signaling.

We examined the ROCK expression in 3T3-L1 cells by Western blot analysis. Both ROCK isoforms are expressed during the course of adipogenesis. A previous study showed that ROCK-II was expressed in 3T3-L1 mature adipocytes (36) while the expression of ROCK-I has not been reported.

Next, we examined the effects of ROCK inhibitors on lipid accumulation in 3T3-L1 cells. We found that two ROCK inhibitors, Y-27632 and fasudil, enhance lipid accumulation, respectively. These findings suggest that inhibition of ROCK enhances adipogenesis. We also assessed when Y-27632 affects adipogenesis. Supplementation with Y-27632 during days 0–4 fully enhances adipogenesis. These results let us speculate that inhibition of ROCK enhances the expression of adipogenic transcription factors. As expected, Y-27632 enhances the expression of adipogenic transcription factors, C/EBPβ, C/EBPα, and PPARγ in the presence of dexamethasone and IBMX, which indicates that inhibition of ROCK enhances adipogenesis through the up-regulation of adipogenic transcription factors. Following this, Y-27632 enhances the expression of adipogenic late markers, such as aP2 and adiponectin.

We assessed the effects of LPA and Y-27632 on adipogenesis and actin cytoskeleton. Because the Rho-ROCK pathway regulates actin cytoskeleton, we examined the effects of LPA and Y-27632 on actin cytoskeleton with phalloidin staining. We showed that stress fiber formation is augmented by LPA and that it is inhibited by Y-27632 in 3T3-L1 preadipocytes. These results provide the evidence that LPA activates the Rho-ROCK pathway and Y-27632 inhibits the pathway. Then, we showed that LPA inhibits adipogenesis in 3T3-L1 cells consistent with a previous report in 3T3-F442A cells. Furthermore, we showed that Y-27632 restores its inhibition in a dose-dependent manner. These results indicate that the Rho-ROCK pathway plays an important role in adipogenesis.

To determine the isoform-specific role of ROCK and to entirely exclude the nonspecific effects of ROCK inhibitors, we examined adipogenesis of ROCK-I (−/−) and ROCK-II (−/−) MEFs. We demonstrated that targeted disruption of ROCK-II enhances adipogenesis and that, in contrast, that of ROCK-I does not enhance adipogenesis. Furthermore, Y-27632 enhances lipid accumulation in ROCK-I (−/−) MEFs and does not enhance lipid accumulation in ROCK-II (−/−) MEFs. It suggests that inhibition of endogenous ROCK-II enhances adipogenesis. In 3T3-L1 cells, we examined the effect of knockdown of ROCK-I or ROCK-II on adipogenesis using siRNA. We showed that ROCK-II siRNA enhances the expression of adipogenic transcription factors while ROCK-I siRNA does not enhance it. Taken together, our results from the pharmacological and genetic approaches indicate that inhibition of ROCK, especially ROCK-II, enhances adipogenesis.

We investigated the mechanisms of the enhancement of adipogenesis by inhibition of ROCK. We demonstrated that Y-27632 inhibits IRS-1 serine phosphorylation and markedly

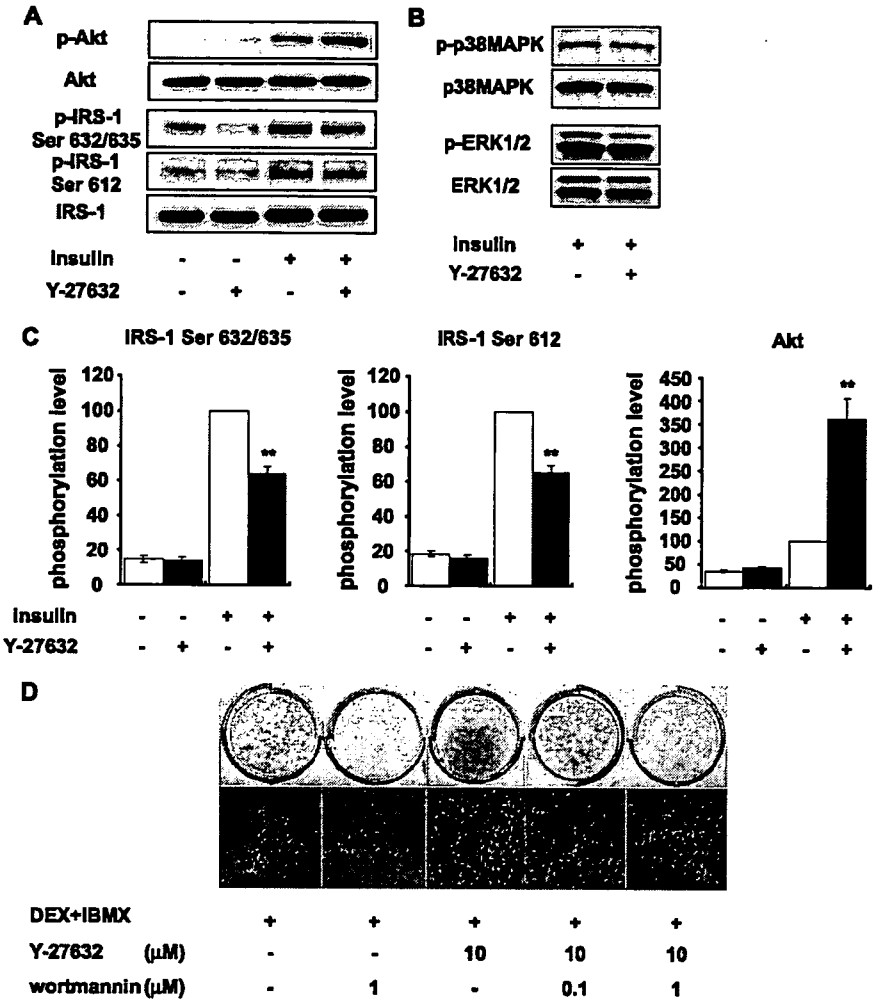

FIGURE 8. **Effect of inhibition of ROCK on intracellular signaling pathway in 3T3-L1 cells.** *A*, effect of Y-27632 on insulin signaling pathway. 3T3-L1 preadipocytes were stimulated with 10 nM insulin for 15 min or 100 nM insulin for 5 min in the absence or presence of 30 μM Y-27632. Western blot analysis was performed using antibodies against phospho-IRS-1 ($Ser^{632/635}$), phospho-IRS-1 (Ser^{612}), IRS-1, phospho-Akt (Ser^{473}), and Akt. All data are representatives of at least three independent experiments. *B*, effect of Y-27632 on MAPK signaling pathway. 3T3-L1 preadipocytes were stimulated with 100 nM insulin for 5 min in the absence or presence of 30 μM Y-27632. Western blot analysis was performed using antibodies against phospho-ERK1/2, ERK1/2, phospho-p38MAPK and p38MAPK. All data are representatives of at least three independent experiments. *C*, quantification of IRS-1 $Ser^{632/635}$ phosphorylation, IRS-1 Ser^{612} phosphorylation, and Akt phosphorylation. Phosphorylation level was normalized to total IRS-1 or total Akt level. Data are expressed as mean ± S.E. from triplicate experiments. **, $p < 0.01$ (Student's *t* test) compared with insulin-stimulated group without Y-27632. *Open bars* are treated without Y-27632. *D*, effect of wortmannin on the enhancement of 3T3-L1 adipogenesis induced by Y-27632. Differentiated adipocytes were fixed and stained with Oil Red O at day 8. Macroscopic and microscopic pictures of cells are shown.

enhances Akt phosphorylation upon the stimulation of insulin in 3T3-L1 preadipocytes. Previously, it has been reported that insulin/IGF-1 signaling is required for adipogenesis. MEFs derived from IRS-1 (−/−) mice do not have enough differentiation properties (27). IRS-1 and IRS-3 double knock-out mice exhibit lipodystrophy (38). Constitutively active Akt causes spontaneous differentiation in 3T3-L1 cells (39). Furthermore, we also demonstrated that an inhibitor of PI3-kinase, wortmannin, blocks the enhancement of adipogenesis induced by Y-27632. Therefore, augmentation of insulin signaling may contribute to the enhancement of preadipocyte differentiation. Concerning MAPK signaling, we showed that Y-27632 slightly enhances p38MAPK phosphorylation and slightly inhibits ERK1/2 phosphorylation in this cell line. Regarding ERK1/2 and p38MAPK, a great deal of evidence about the molecular link between MAPK and adipogenesis has been accumulating (40–45). However, their roles in adipogenesis are still controversial. In addition to pharmacological approaches, we showed that in ROCK-II (−/−) MEFs and even in ROCK-II (+/−) MEFs, insulin-induced Akt phosphorylation is enhanced compared with that in wild-type MEFs while in ROCK-I MEFs, there is no significant difference in insulin-induced Akt phosphorylation between each genotype. It provides the direct evidence that loss of ROCK-II enhances insulin-induced Akt phosphorylation.

Regarding the ROCK and insulin signaling, we showed that a ROCK inhibitor reduces IRS-1 serine phosphorylation and increases Akt phosphorylation in 3T3-L1 preadipocytes. It is known that ROCK directly associates with IRS-1 and phosphorylates its serine residues (35–37). In addition, previous studies have reported that IRS-1 serine phosphorylation negatively regulates insulin signaling in vascular smooth muscle cells (37) and NIH3T3 fibroblasts (46). However, recently, it has been reported that ROCK phosphorylates IRS-1 serine residues and positively regulates insulin signaling in 3T3-L1 mature adipocytes (36). The discrepancy between these reports shows that IRS-1 serine phosphorylation regulates insulin signaling differently depending on cell types. Therefore, there could be a difference in the regulation of insulin signaling by IRS-1 serine phosphorylation between preadipocytes and mature adipocytes.

Adipogenic analysis of both ROCK-I (−/−) and ROCK-II (−/−) MEFs revealed that loss of ROCK-II, not ROCK-I, enhances adipogenesis. The isoform-specific role of ROCK has been still obscure both *in vitro* and *in vivo*. As previously reported, loss of ROCK-I results in the eyelid open at birth (EOB) and omphalocele, while loss of ROCK-II results in placental dysfunction, intrauterine growth retardation, and fetal death. However, recently it has been reported that ROCK-II knock-out mice backcrossed in the C57BL6/N background exhibit not only the placental phenotype but also EOB and omphalocele (47). Concerning actin cytoskeletal regulation, it

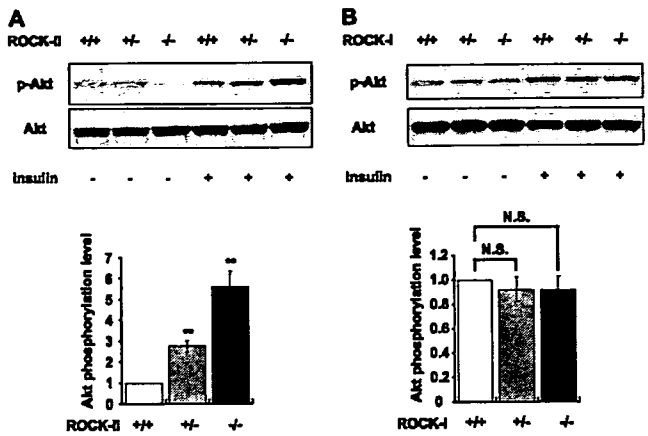

FIGURE 9. **Effect of knock-out of ROCK on insulin-induced Akt phosphorylation in MEFs.** *A*, insulin-induced Akt phosphorylation in ROCK-II (−/−) MEFs. ROCK-II (+/+), (+/−), and (−/−) MEFs were stimulated with 100 nM insulin for 5 min after serum starvation. Western blot analysis was performed using antibodies against phospho-Akt (Ser^{473}) and Akt. All data are representatives of at least three independent experiments. Quantification of insulin-induced Akt phosphorylation. Phospho-Akt level was normalized to total Akt level. Data are expressed as mean ± S.E. from triplicate experiments. **, $p < 0.01$ (Student's *t* test) compared with ROCK-II (+/+) MEFs. *B*, insulin-induced Akt phosphorylation in ROCK-I (−/−) MEFs. ROCK-I (+/+), (+/−), and (−/−) MEFs were stimulated with 100 nM insulin for 15 min after serum starvation. Western blot analysis was performed using antibodies against phospho-Akt (Ser^{473}) and Akt. All data are representatives of at least three independent experiments. Quantification of insulin-induced Akt phosphorylation. Phospho-Akt level was normalized to total Akt level. Data are expressed as mean ± S.E. from triplicate experiments. *N.S.*, not significant.

suggests that ROCK-I and ROCK-II cooperatively regulate actin bundle assembly required for eyelid and ventral body wall closure. In this context, our findings that inhibition of ROCK-II, not ROCK-I, enhances adipogenesis is a novel isoform-specific role of ROCK.

In summary, the present study first provides the robust and direct evidence that inhibition of ROCK-II enhances adipogenesis accompanied by the up-regulation of adipogenic transcription factors and that inhibition of ROCK-II enhances insulin-induced Akt phosphorylation. These results indicate that inhibition of ROCK-II enhances adipogenesis, at least in part, via augmentation of insulin signaling. Finally, these findings raise the possibility that ROCK-II is a novel target for the treatment of obesity, insulin resistance, and type 2 diabetes.

REFERENCES

1. Spiegelman, B. M., and Flier, J. S. (2001) *Cell* **104,** 531–543
2. Flier, J. S. (2004) *Cell* **116,** 337–350
3. Hwang, C. S., Loftus, T. M., Mandrup, S., and Lane, M. D. (1997) *Annu. Rev. Cell Dev. Biol.* **13,** 231–259
4. Rosen, E. D., and Spiegelman, B. M. (2000) *Annu. Rev. Cell Dev. Biol.* **16,** 145–171
5. Cao, Z., Umek, R. M., and McKnight, S. L. (1991) *Genes Dev.* **5,** 1538–1552
6. Tontonoz, P., Hu, E., Graves, R. A., Budavari, A. I., and Spiegelman, B. M. (1994) *Genes Dev.* **8,** 1224–1234
7. Lane, M. D., Tang, Q. Q., and Jiang, M. S. (1999) *Biochem. Biophys. Res. Commun.* **266,** 677–683
8. Wu, Z., Rosen, E. D., Brun, R., Hauser, S., Adelmant, G., Troy, A. E., McKeon, C., Darlington, G. J., and Spiegelman, B. M. (1999) *Mol. Cell* **3,** 151–158
9. Jaffe, A. B., and Hall, A. (2005) *Annu. Rev. Cell Dev. Biol.* **21,** 247–269
10. Kanzaki, M., and Pessin, J. E. (2001) *J. Biol. Chem.* **276,** 42436–42444
11. Etienne-Manneville, S., and Hall, A. (2002) *Nature* **420,** 629–635
12. Riento, K., and Ridley, A. J. (2003) *Nat. Rev. Mol. Cell. Biol.* **4,** 446–456
13. Leung, T., Chen, X. Q., Manser, E., and Lim, L. (1996) *Mol. Cell. Biol.* **16,** 5313–5327
14. Leung, T., Manser, E., Tan, L., and Lim, L. (1995) *J. Biol. Chem.* **270,** 29051–29054
15. Ishizaki, T., Maekawa, M., Fujisawa, K., Okawa, K., Iwamatsu, A., Fujita, A., Watanabe, N., Saito, Y., Kakizuka, A., Morii, N., and Narumiya, S. (1996) *EMBO J.* **15,** 1885–1893
16. Matsui, T., Amano, M., Yamamoto, T., Chihara, K., Nakafuku, M., Ito, M., Nakano, T., Okawa, K., Iwamatsu, A., and Kaibuchi, K. (1996) *EMBO J.* **15,** 2208–2216
17. Uehata, M., Ishizaki, T., Satoh, H., Ono, T., Kawahara, T., Morishita, T., Tamakawa, H., Yamagami, K., Inui, J., Maekawa, M., and Narumiya, S. (1997) *Nature* **389,** 990–994
18. Itoh, K., Yoshioka, K., Akedo, H., Uehata, M., Ishizaki, T., and Narumiya, S. (1999) *Nat. Med.* **5,** 221–225
19. Shimokawa, H., Seto, M., Katsumata, N., Amano, M., Kozai, T., Yamawaki, T., Kuwata, K., Kandabashi, T., Egashira, K., Ikegaki, I., Asano, T., Kaibuchi, K., and Takeshita, A. (1999) *Cardiovasc. Res.* **43,** 1029–1039
20. Sawada, N., Itoh, H., Ueyama, K., Yamashita, J., Doi, K., Chun, T. H., Inoue, M., Masatsugu, K., Saito, T., Fukunaga, Y., Sakaguchi, S., Arai, H., Ohno, N., Komeda, M., and Nakao, K. (2000) *Circulation* **101,** 2030–2033
21. Sordella, R., Jiang, W., Chen, G. C., Curto, M., and Settleman, J. (2003) *Cell* **113,** 147–158
22. McBeath, R., Pirone, D. M., Nelson, C. M., Bhadriraju, K., and Chen, C. S. (2004) *Dev. Cell* **6,** 483–495
23. Frost, S. C., and Lane, M. D. (1985) *J. Biol. Chem.* **260,** 2646–2652
24. Ramirez-Zacarias, J. L., Castro-Munozledo, F., and Kuri-Harcuch, W. (1992) *Histochemistry* **97,** 493–497
25. Shimizu, Y., Thumkeo, D., Keel, J., Ishizaki, T., Oshima, H., Oshima, M., Noda, Y., Matsumura, F., Taketo, M. M., and Narumiya, S. (2005) *J. Cell Biol.* **168,** 941–953
26. Thumkeo, D., Keel, J., Ishizaki, T., Hirose, M., Nonomura, K., Oshima, H., Oshima, M., Taketo, M. M., and Narumiya, S. (2003) *Mol. Cell. Biol.* **23,** 5043–5055
27. Miki, H., Yamauchi, T., Suzuki, R., Komeda, K., Tsuchida, A., Kubota, N., Terauchi, Y., Kamon, J., Kaburagi, Y., Matsui, J., Akanuma, Y., Nagai, R., Kimura, S., Tobe, K., and Kadowaki, T. (2001) *Mol. Cell. Biol.* **21,** 2521–2532
28. Sandouk, T., Reda, D., and Hofmann, C. (1993) *Am. J. Physiol.* **264,** C1600–C1608
29. Norisada, N., Masuzaki, H., Fujimoto, M., Inoue, G., Hosoda, K., Hayashi, T., Watanabe, M., Muraoka, S., Yoneda, F., and Nakao, K. (2004) *Metabolism* **53,** 1532–1537
30. Kletzien, R. F., Clarke, S. D., and Ulrich, R. G. (1992) *Mol. Pharmacol.* **41,** 393–398
31. Rosen, E. D., Walkey, C. J., Puigserver, P., and Spiegelman, B. M. (2000) *Genes Dev.* **14,** 1293–1307
32. Simon, M. F., Daviaud, D., Pradere, J. P., Gres, S., Guigne, C., Wabitsch, M., Chun, J., Valet, P., and Saulnier-Blache, J. S. (2005) *J. Biol. Chem.* **280,** 14656–14662
33. Tsuji, T., Ishizaki, T., Okamoto, M., Higashida, C., Kimura, K., Furuyashiki, T., Arakawa, Y., Birge, R. B., Nakamoto, T., Hirai, H., and Narumiya, S. (2002) *J. Cell Biol.* **157,** 819–830
34. Ridley, A. J., and Hall, A. (1992) *Cell* **70,** 389–399
35. Farah, S., Agazie, Y., Ohan, N., Ngsee, J. K., and Liu, X. J. (1998) *J. Biol. Chem.* **273,** 4740–4746
36. Furukawa, N., Ongusaha, P., Jahng, W. J., Araki, K., Choi, C. S., Kim, H. J., Lee, Y. H., Kaibuchi, K., Kahn, B. B., Masuzaki, H., Kim, J. K., Lee, S. W., and Kim, Y. B. (2005) *Cell Metab.* **2,** 119–129
37. Begum, N., Sandu, O. A., Ito, M., Lohmann, S. M., and Smolenski, A. (2002) *J. Biol. Chem.* **277,** 6214–6222
38. Laustsen, P. G., Michael, M. D., Crute, B. E., Cohen, S. E., Ueki, K., Kulkarni, R. N., Keller, S. R., Lienhard, G. E., and Kahn, C. R. (2002) *Genes Dev.* **16,** 3213–3222
39. Kohn, A. D., Summers, S. A., Birnbaum, M. J., and Roth, R. A. (1996) *J. Biol. Chem.* **271,** 31372–31378

40. Belmonte, N., Phillips, B. W., Massiera, F., Villageois, P., Wdziekonski, B., Saint-Marc, P., Nichols, J., Aubert, J., Saeki, K., Yuo, A., Narumiya, S., Ailhaud, G., and Dani, C. (2001) *Mol. Endocrinol.* **15,** 2037–2049
41. Benito, M., Porras, A., Nebreda, A. R., and Santos, E. (1991) *Science* **253,** 565–568
42. Camp, H. S., and Tafuri, S. R. (1997) *J. Biol. Chem.* **272,** 10811–10816
43. Engelman, J. A., Lisanti, M. P., and Scherer, P. E. (1998) *J. Biol. Chem.* **273,** 32111–32120
44. Hu, E., Kim, J. B., Sarraf, P., and Spiegelman, B. M. (1996) *Science* **274,** 2100–2103
45. Prusty, D., Park, B. H., Davis, K. E., and Farmer, S. R. (2002) *J. Biol. Chem.* **277,** 46226–46232
46. Ozes, O. N., Akca, H., Mayo, L. D., Gustin, J. A., Maehama, T., Dixon, J. E., and Donner, D. B. (2001) *Proc. Natl. Acad. Sci. U. S. A.* **98,** 4640–4645
47. Thumkeo, D., Shimizu, Y., Sakamoto, S., Yamada, S., and Narumiya, S. (2005) *Genes Cells* **10,** 825–834

0013-7227/07/$15.00/0
Printed in U.S.A.

Endocrinology 148(11):5268–5277

doi: 10.1210/en.2007-0349

Ceramide and Adenosine 5′-Monophosphate-Activated Protein Kinase Are Two Novel Regulators of 11β-Hydroxysteroid Dehydrogenase Type 1 Expression and Activity in Cultured Preadipocytes

N. Arai, H. Masuzaki, T. Tanaka, T. Ishii, S. Yasue, N. Kobayashi, T. Tomita, M. Noguchi, T. Kusakabe, J. Fujikura, K. Ebihara, M. Hirata, K. Hosoda, T. Hayashi, H. Sawai, Y. Minokoshi, and K. Nakao

Division of Endocrinology and Metabolism (N.A., H.M., T.Ta., T.I., S.Y., N.K., T.To., M.N., T.K., J.F., K.E., M.H., K.H., K.N.), Department of Medicine and Clinical Science, Kyoto University Graduate School of Medicine, Kyoto 606-8507, Japan; Department of Human Coexistence (T.H.), Kyoto University Graduate School of Human and Environmental Studies, Kyoto 606-8501, Japan; Department of Internal Medicine (H.S.), Osaka Dental University, Osaka 573-1121, Japan; and Department of Developmental Physiology (Y.M.), National Institute for Physiological Science, Aichi 444-8585, Japan

Increased activity of intracellular glucocorticoid reactivating enzyme, 11β-hydroxysteroid dehydrogenase type 1 (11β-HSD1) in obese adipose tissue contributes to adipose dysfunction. As recent studies have highlighted a potential role of preadipocytes in adipose dysfunction, we tested the hypothesis that a variety of metabolic stress mediated by ceramide or AMP-activated protein kinase (AMPK) would regulate 11β-HSD1 in preadipocytes. The present study is the first to show that 1) expression of 11β-HSD1 in 3T3-L1 preadipocytes was robustly induced when cells were treated with cell-permeable ceramide analogue C_2 ceramide, bacterial sphingomyelinase, and sphingosine 1-phosphate, 2) 5-aminoimidazole-4-carboxamide ribonucleoside (AICAR)-induced activation of AMPK augmented the expression and enzyme activity of 11β-HSD1, and 3) these results were reproduced in human preadipocytes. We demonstrate for the first time that C_2 ceramide and AICAR markedly induced the expression of CCAAT/enhancer-binding protein (C/EBP) β and its binding to 11β-HSD1 promoter. Transient knockdown of C/EBPβ protein by small interfering RNA markedly attenuated the expression of 11β-HSD1 induced by C_2 ceramide or AICAR. The present study provides novel evidence that ceramide- and AMPK-mediated signaling pathways augment the expression and activity of 11β-HSD1 in preadipocytes by way of C/EBPβ, thereby highlighting a novel, metabolic stress-related regulation of 11β-HSD1 in a cell-specific manner. (*Endocrinology* 148: 5268–5277, 2007)

METABOLIC SYNDROME IS characterized by a cluster of glucose intolerance, hypertension, and dyslipidemia on a basis of insulin resistance and excess in intraabdominal fat accumulation (1–3). Functional abnormalities of adipose tissue have been implicated in the pathophysiology of metabolic syndrome (2). A series of transgenic and knockout experiments in mouse models suggest that exaggerated reactivation of glucocorticoid in adipose tissue, mediated by enzyme 11β-hydroxysteroid dehydrogenase type 1 (11β-HSD1), contributes to dysfunction of adipose tissue (3–7). 11β-HSD1 is a bidirectional (oxo-reductase and dehydrogenase) enzyme (8), expressing abundantly in adipose tissue, liver, and central nervous system (9, 10). Notably, 11β-HSD1 mainly acts as an oxo-reductase *in vivo* and reactivates inactive cortisone into active cortisol (8). Transgenic mice overexpressing 11β-HSD1 in adipose tissue exemplified major phenotype of metabolic syndrome (3, 4), whereas systemic 11β-HSD1 knockout mice were protected against diabetes and dyslipidemia on a high-fat diet (5–7). These data suggest that an increased level of adipose 11β-HSD1 considerably contributes to metabolic derangement. Consistent with this notion, selective 11β-HSD1 inhibitors are shown to ameliorate diabetes, dyslipidemia, and arteriosclerosis in experimental murine models (11, 12).

Obese adipose tissue is subjected to multiple cellular stresses such as endoplasmic reticulum stress and oxidative stress (13). Local hypoxia, tissue dysnutrition, and resultant cell death are potentially linked to macrophage recruitment and local inflammation in adipose tissue (13, 14). Recent studies also highlight a complexity of preadipocytes in controlling adipose tissue function (15, 16). Nevertheless mature adipocytes are the major component of adipose tissue and predominant source of 11β-HSD1 (10, 17); a considerable amount of 11β-HSD1 expression is also detected in stromal-vascular cells from adipose tissue (17). The underlying mechanism whereby 11β-HSD1 is elevated in obese adipose tissue still remains obscure, and the regulation of 11β-HSD1 in preadipocytes has been poorly understood.

In this context, we hypothesized that a variety of metabolic stresses would regulate the expression of 11β-HSD1 in preadipocytes. The sphingolipid ceramide serves as a bioactive lipid mediator in response to a variety of metabolic stresses

First Published Online August 16, 2007

Abbreviations: ACC, Acetyl-CoA carboxylase; AICAR, 5-aminoimidazole-4-carboxamide ribonucleosides; AMPK, AMP-activated protein kinase; C/EBP, CCAAT/enhancer-binding protein; ChIP, chromatin immunoprecipitation; 11β-HSD1, 11β-hydroxysteroid dehydronenase type 1; MCP-1, monocyte chemoattractant protein-1; Pref-1, preadipocyte factor-1; SMase, sphingomyelinase; S1P, sphingosine 1-phosphate; siRNA, small interfering RNA.

Endocrinology is published monthly by The Endocrine Society (http://www.endo-society.org), the foremost professional society serving the endocrine community.

including inflammation and oxidative stress (18). Ceramide is generated by *de novo* synthesis as well as hydrolysis of membrane sphingomyelin by sphingomyelinase (SMase) (18, 19). Ceramide and its metabolites, sphingosine and sphingosine 1-phosphate (S1P), mediate a variety of biological events such as apoptosis, cell growth, and the stress response (18, 19). In contrast, AMP-activated protein kinase (AMPK) is another mediator of metabolic stress that responds to the negative energy balance within cells (20–22). AMPK is activated by stresses that increase intracellular AMP level such as local hypoxia, glucose deprivation, and ischemia (21). Whereas the function of AMPK in liver and muscle has been well investigated, its role in adipose tissue still remains obscure (23, 24). In the present study, using murine 3T3-L1 preadipocytes and human preadipocytes, we investigated the effect of ceramide- and AMPK-mediated signaling pathways on the expression of 11β-HSD1.

Materials and Methods

Reagents and chemicals

5-Aminoimidazole-4-carboxamide ribonucleoside (AICAR) was obtained from Toronto Research Chemicals (Toronto, Canada). A selective AMPK inhibitor, Compound C, and C_2 ceramide (*N*-acetyl-sphingosine) were purchased from Carbiochem (San Diego, CA). Bacterial SMase and S1P were from Sigma Chemicals (St. Louis, MO). Antibodies against phospho (Ser 79) acetyl-CoA carboxylase (ACC), CCAAT/enhancer-binding protein (C/EBP) β, and β-actin were from Upstate Biotechnology (Lake Placid, NY), Affinity BioReagents Inc. (Golden, CO), and Sigma Chemicals.

Cell culture and treatment

3T3-L1 fibrobrasts (kindly provided from Dr. H. Green and Dr. M. Morikawa, Harvard Medical School, Boston, MA) were maintained in DMEM containing 10% (vol/vol) calf serum at 37 C in 10% CO_2. Human perirenal preadipocytes were purchased from Cambrex (Walkersville, MD) (25, 26) and maintained according to the manufacturer's instructions. For differentiation of 3T3-L1 preadipocytes into mature adipocytes, cells (2 d postconfluence) were incubated with DMEM containing 10% (vol/vol) fetal bovine serum, 0.5 mM 3-isobutyl-1-methylxanthine, 0.25 μM dexamethasone, and 1 μg/ml insulin for 2 d, followed by another 2-d incubation with DMEM containing FBS and insulin (27). Additional incubation with DMEM containing FBS for 4 d completes the differentiation. Compound C and C_2 ceramide were dissolved in DMSO and added to the media within 0.1% of volume. S1P was dissolved in water containing 0.4% BSA and added to the media within 1.0% of volume.

RNA preparation and quantitative real-time PCR

Total RNA was extracted from cultured cells using TRIzol Reagent (Invitrogen, Carlsbad, CA), and cDNA was then synthesized using iScript cDNA Synthesis Kit (Bio-Rad, Hercules, CA) according to the manufacturer's instructions. To determine the mRNA levels, probes and primers were employed as follows: probe (5′FAM-tccgagttcaaggcagcgagacactacc-TAMRA-3′), forward (5′-ccaggtcggaggaaggtctc-3′), and reverse (5′-ccagcaatgtagtgagcagagg-3′) for murine 11β-HSD1; probe (5′FAM-ccccactcacctgctgctactcattca-TAMRA-3′), forward (5′-ttggctcagccagatgca-3′), and reverse (5′-ccagcctactcattgggatca-3′) for murine monocyte chemoattractant protein-1 (MCP-1); probe (5′FAM-acattgtcagcctcgcagaatccatactg-TAMRA-3′), forward (5′-atgcgacccaccctgtgac-3′), and reverse (5′-gaccctcccagccaacatg-3′) for murine preadipocyte factor-1 (Pref-1); and probe (5′-cattgttgtcgtctcctctctggctggg-3′), forward (5′-ttgcccatgctgaagcagag-3′), and reverse (5′-gcaaccattggataagccactt-3′) for human 11β-HSD1. TaqMan PCR was performed using ABI Prism 7700 Sequence Detection System as instructed by the manufacturer (Applied Biosystems, Foster City, CA). Each value of mRNA level was normalized to that of 18S rRNA.

Western blot analysis

Cells were washed twice with ice-cold PBS, and harvested in lysis buffer [40 mM HEPES, 10 mM EDTA, 100 mM NaF, 10 mM sodium pyrophosphate, 1 mM Na_3VO_4, 0.1 mg/ml aprotinin, 1 mM PMSF, 50 nM okadaic acid, and 1% (vol/vol) Nonidet P-40 at pH 7.5]. For analysis of C/EBPβ, cells were harvested in lysis buffer [1% (wt/vol) SDS, 60 mM Tris-HCl, 1 mM Na_3VO_4, 0.1 mg/ml aprotinin, 1 mM PMSF and 50 nM okadaic acid at pH 6.8], and boiled at 100 C for 10 min. After centrifugation, supernatants were normalized for protein concentration via Bradford method and then equal amounts of protein were subjected to SDS-PAGE and immunoblot.

Measurement of AMPK activity

Activation of AMPK is assessed by the immunoblot of Thr172-phosphorylated AMPKα. Antibodies against AMPKα and phosphorylated (Thr172) AMPK (Cell Signaling Technology, Beverly, MA) can detect both α1 and α2 isoform of the catalytic subunit (28). In 3T3-L1 adipocytes, AMPK activity is largely attributable to the α1 isoform (29), and both α1 and α2 catalytic subunit isoforms are activated by AICAR (29). The phosphorylation at Thr172 parallels the degree of AMPK activation, thus making it possible to estimate the activity of both isoform complexes (28).

Measurement of 11β-HSD1 activity

Assays for 11β-HSD1 activity were performed by incubating viable cells with 250 nM corticosteroids with appropriate tritium-labeled tracer. In assays for oxo-reductase activity, cells were incubated in serum-free DMEM containing 250 nM cortisone that includes 6.4 μCi/ml tritium-labeled tracer [1,2-^{3}H]$_2$ cortisone (Muromachi Yakuhin LTD, Kyoto, Japan). In assays for dehydrogenase activity, cells were incubated in serum-free DMEM containing 250 nM cortisol with 6.4 μCi/ml tritium-labeled tracer [1,2,6,7-^{3}H]$_4$ cortisol (Muromachi Yakuhin LTD). After the incubation at 37 C for indicated time, corticosteroids were extracted by ethyl acetate, separated by thin-layer chromatography in chloroform: methanol (95:5), and quantified by autoradiography. As a control (indicated as ref.), serum-free DMEM with tritium-labeled cortisone or cortisol was incubated without cells.

Chromatin immunoprecipitation (ChIP) analysis

ChIP analysis was performed using an assay kit (Upstate Biotechnology) according to the manufacturer's protocol. Anti-C/EBPβ antibody used for immunoprecipitation is from Santa Cruz Biotechnology (Santa Cruz, CA). Forward primer (5′-ctggaagttgcctcttactc-3′) and reverse primer (5′-cctgtaggacacacgaagaa-3′) were used to amplify the DNA fragment between −170 and +71 (relative to the transcription start site) of mouse 11β-HSD1 genomic DNA, which contains two putative C/EBP binding sites (30).

RNA interference (RNAi)

Two Stealth RNAi for mouse C/EBPβ were obtained (Invitrogen). Each small interfering RNA (siRNA), termed RNAi154 and RNAi168, was designed as a 25-bp duplex oligoribonucleotide with a sense strand corresponding to nucleotides 154–173 or 168–192 of the reported mouse C/EBPβ coding sequence (GenBank accession no. NM009883), respectively. The Stealth RNAi negative control duplex (Invitrogen) was used as a control oligoribonucleotide. According to the manufacturer's protocol, 3T3-L1 preadipocytes were transfected with 10 nM siRNA in antibiotic-free medium using Lipofectamine RNAiMAX (Invitrogen). The transfected cells were cultured overnight and applied to the experiments.

Statistical analysis

The data are presented as means ± SEM from independent three or four experiments. Student's *t* test was used to compare the data when the variances of two groups were regarded equal (within 5%). When variances of two groups were apparently different, Welch's *t* test was used. Differences were accepted as significant at $P < 0.05$ level.

Results

When 3T3-L1 preadipocytes were differentiated into mature adipocytes, the level of 11β-HSD1 mRNA was increased by 150-fold (Fig. 1). Based on this result, we first analyzed the effect of ceramide signaling on the expression of 11β-HSD1 in both 3T3-L1 preadipocytes and differentiated adipocytes.

Effect of ceramide on the expression of 11β-HSD1 in 3T3-L1 preadipocytes

When 3T3-L1 preadipocytes were treated with a short chain ceramide analog, C_2 ceramide (10–100 μM), for 24 h, mRNA of Pref-1, which is known to express abundantly in preadipocytes (31, 32), was not altered (Fig. 2A). In contrast, expression of MCP-1 and 11β-HSD1 was induced dose-dependently, reaching to 2.0 ± 0.1-fold ($P < 0.01$) and 2.2 ± 0.1-fold ($P < 0.01$), respectively (Fig. 2, B and C). To evaluate the effect of C_2 ceramide on the 11β-HSD1 enzyme activity, cells were incubated with tritium-labeled cortisone or cortisol. C_2 ceramide significantly increased the conversion of cortisone to cortisol by 1.7 ± 0.1-fold ($P < 0.05$) (Fig. 2D, *left*). This indicates that 11β-HSD1 oxo-reductase activity was increased in response to C_2 ceramide. In contrast, 11β-HSD1 dehydrogenase activity was neither detected nor induced during a 24-h incubation period (Fig. 2D, *right*). These results indicate that 11β-HSD1 in 3T3-L1 preadipocytes acts solely as an oxo-reductase.

Hydrolysis of membrane sphingomyelin by SMase provoke intracellular accumulation of ceramide (19). Ceramide is subsequently metabolized to sphingosine and S1P, both of which mediate biological events including cell growth and apoptosis (19). We thus treated 3T3-L1 preadipocytes with bacterial SMase and S1P. When cells were treated with bacterial SMase (25–200 mU/ml) and S1P (1.0–10 μM), 11β-HSD1 mRNA level was significantly induced, reaching to 1.7 ± 0.2-fold ($P < 0.05$) and 3.0 ± 0.5-fold ($P < 0.05$), respectively (Fig. 2, E and F). To further investigate whether ceramide signaling would be involved in the induction of 11β-HSD1 by inflammatory cytokines, inhibitors of ceramide [fumonisin B1, an inhibitor of ceramide synthase (33); myriocin, an inhibitor of serine palmitoyltransferase (34); desipramine, an inhibitor of SMase (35)] were cotreated with 3T3-L1 preadipocytes. Desipramine (10 and 20 μM) dose-dependently attenuated the expression of 11β-HSD1 mRNA induced by TNFα or IL-1β [46 ± 10% ($P = 0.07$) and 41 ± 2% ($P < 0.01$), respectively]. This result indicates that induction of 11β-HSD1 by TNFα or IL-1β, at least in part, is attributable to the activation of SMase. Such an effect was not observed when treated with fumonisin B1 or myriocin (data not shown). These results raise a possibility that ceramide-mediated signaling pathway is involved in the regulation of 11β-HSD1 in preadipocytes.

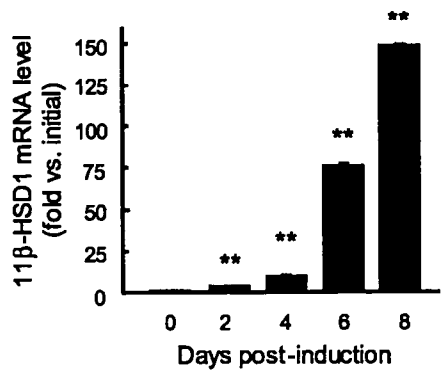

FIG. 1. Expression profile of 11β-HSD1 mRNA during the course of differentiation in 3T3-L1 cells. Postconfluent 3T3-L1 preadipocytes were induced to differentiate as described in *Materials and Methods*. mRNA level of 11β-HSD1 was determined. Results are means ± SEM from three experiments. **, $P < 0.01$ compared with 2 d postconfluent preadipocytes (initial).

Effect of ceramide on the expression of 11β-HSD1 in 3T3-L1 differentiated adipocytes

Induction of 11β-HSD1 mRNA by C_2 ceramide (10–100 μM) was not observed in 3T3-L1 differentiated adipocytes during 24-h incubation periods (Fig. 3A). Similarly, SMase (25–200 mU/ml) and S1P (1.0–10 μM) did not induce the expression of 11β-HSD1 (Fig. 3, B and C). These results are in agreement with our data that a robust induction of 11β-HSD1 expression by TNFα and IL-1β was observed only in 3T3-L1 preadipocytes but not in differentiated adipocytes (data not shown). Altogether, our data suggest that the effect of C_2 ceramide, SMase, and S1P on 11β-HSD1 expression is restricted in preadipocytes.

Effect of AICAR on the expression of 11β-HSD1 in 3T3-L1 preadipocytes

AMPK is activated by cellular stresses that interfere with ATP production (20–22). In contrast, 11β-HSD1 is a NADPH-dependent enzyme and its oxo-reductase activity requires NADPH supply from a glucose metabolizing pathway (36). This scheme tempted us to speculate that 11β-HSD1 would be involved in an AMPK-mediated fuel sensing mechanism. To test this hypothesis, we examined the effect of AMPK on the expression of 11β-HSD1 using a cell permeable AMP analog, AICAR (37).

When 3T3-L1 preadipocytes were treated with AICAR (0.1–0.5 mM) for 24 h, AMPK phosphorylation was increased pronouncedly (Fig. 4A). MCP-1 mRNA level was not altered even after the treatment with AICAR (Fig. 4B). In contrast, 11β-HSD1 mRNA level was increased in a dose-dependent manner, reaching to 8.7 ± 0.8-fold ($P < 0.05$) (Fig. 4C). Oxo-reductase activity of 11β-HSD1 was concomitantly increased by 3.0 ± 0.2-fold ($P < 0.01$) after the treatment with 0.5 mM AICAR (Fig. 4D).

To further evaluate the involvement of AMPK in the regulation of 11β-HSD1, cells were cotreated with AICAR and a selective AMPK inhibitor, compound C (38). Western blot analyses showed that augmented phosphorylation of AMPK and ACC by the treatment with 0.5 mM AICAR were attenuated when cells were cotreated with 10 μM compound C (Fig. 5A). Compound C completely blocked the effect of 0.5 mM AICAR on its augmentation of 11β-HSD1 (80 ± 2.4% decrease compared with AICAR-treated group, $P < 0.01$) (Fig. 5B). These results indicate that augmented expression of 11β-HSD1 by AICAR largely is attributable to the activation of AMPK. In contrast, mRNA of glucocorticoid receptor, which is known to express considerably in preadipocytes (39), was not affected by AICAR or compound C (data not shown).

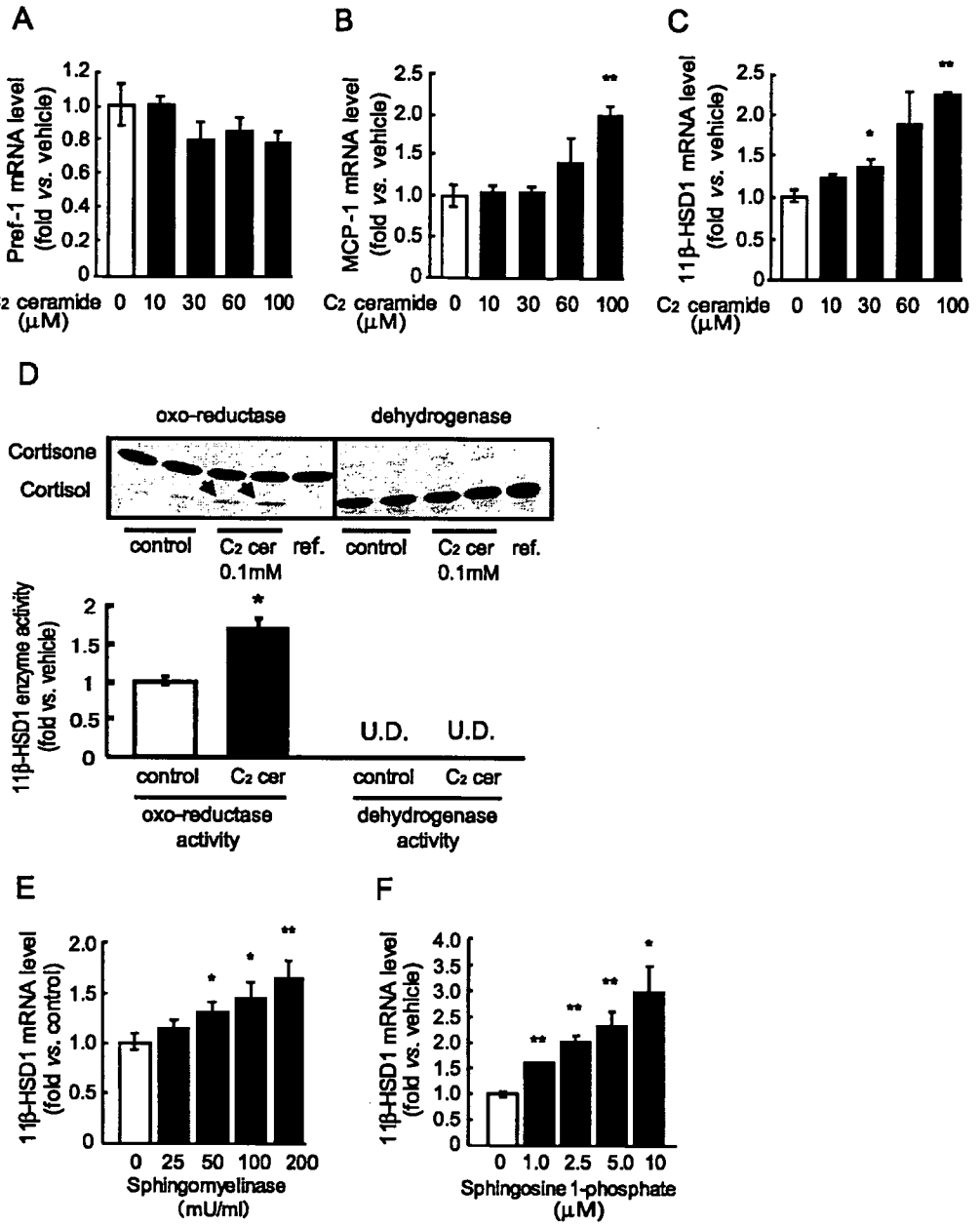

FIG. 2. Ceramide induces the expression of 11β-HSD1 in 3T3-L1 preadipocytes. A–D, Cells were treated with C_2 ceramide (10–100 μM) for 24 h. mRNA level of Pref-1 (A), MCP-1 (B), and 11β-HSD1 (C). D, Assay for 11β-HSD1 enzyme activity. Cells treated with C_2 ceramide (100 μM) for 24 h were subsequently incubated in serum-free media containing 250 nM of cortisone or cortisol with tritium-labeled tracer (6.4 μCi/ml of $[1,2\text{-}^3H]_2$ cortisone or $[1,2,6,7\text{-}^3H]_4$ cortisol) for 12 h. Emerged spots of cortisol are indicated by *arrows*. E and F, mRNA level of 11β-HSD1 after treatment with bacterial SMase (25–200 mU/ml) (E) and S1P (1.0–10 μM) (F) for 24 h. Results are means ± SEM from three experiments. *, $P < 0.05$, **, $P < 0.01$ compared with vehicle-treated group. U.D., Under detectable.

Effects of ceramide and AMPK signaling on the expression of 11β-HSD1 in human preadipocytes

To explore whether potent effects of ceramide and AMPK on 11β-HSD1 expression are reproduced in human preadipocytes (25, 26), impact of C_2 ceramide, S1P, and AICAR on 11β-HSD1 expression and enzyme activity were similarly analyzed. When cells were treated with C_2 ceramide (25–100 μM) for 24 h, 11β-HSD1 mRNA level was increased dose dependently, reaching to 5.3 ± 0.3-fold ($P < 0.01$) (Fig. 6A). In contrast, the effect of S1P (2.5–10 μM) was marginal (Fig. 6A). AICAR (0.3–1.0 mM) induced the phosphorylation of AMPK (Fig. 6B) and augmented 11β-HSD1 mRNA level by 2.8 ± 0.1-fold ($P < 0.01$) (Fig. 6A). C_2 ceramide (50 μM) and AICAR (1.0 mM) significantly increased the oxo-reductase activity of 11β-HSD1 by 2.9 ± 0.3-fold ($P < 0.01$) and 2.1 ± 0.04-fold ($P < 0.05$) (Fig. 6C).

Induction of C/EBPβ by ceramide and AMPK signaling in 3T3-L1 preadipocytes

11β-HSD1 promoter contains a couple of C/EBP binding sites, and C/EBP mediated regulation of 11β-HSD1 has long